Design of the Sensor Pod of the Hypersonic Configurable Unit Ballistic Experiment (HyCUBE)

A THESIS
SUBMITTED TO THE FACULTY OF THE GRADUATE SCHOOL
OF THE UNIVERSITY OF MINNESOTA
BY

Nathaniel Anderson

IN PARTIAL FULFILLMENT OF THE REQUIREMENTS
FOR THE DEGREE OF
MASTER OF SCIENCE

Ellen K. Longmire, Adviser

July, 2021

Acknowledgements

I would like to thank my advisor, Professor Ellen Longmire, for her insight and guidance throughout my time as a graduate student. There were many points during my research where I felt unsure of how to accomplish the task at hand, or even what the next task should be, but Professor Longmire was always willing to help guide my work and tackle each task. I am grateful to have been able to work with her as she always pushed me to put forward my best work and go deeper in each phase of my master's research.

I would to thank Dr. Ioannis Nompelis for being a tremendous resource for whatever questions I had about practically anything and everything. From being an excellent person to discuss simulation results to hand-holding me through setting up remote server access and everything Linux and CFD related, I know I could not have made it through without him.

I would like to thank Alice Loewenson for her contributions to my research through running CFD simulations, creating figures, and proof-reading and writing many article drafts. Alice was always willing to help me out and even go the extra mile, which I greatly appreciated.

I would like to thank the entire HyCUBE team for their hard work on this project. It was truly a pleasure to work with this group of people. I enjoyed the multidisciplinary nature of the team as it was interesting to see the work that was being done on the GNC and systems aspects of HyCUBE, in addition to the fluids aspects, and to see the different perspectives each group brought to the table.

I would like to thank Dr. Marien Simeni Simeni for his insight on reentry plasmas. His expertise was extremely valuable in informing our research from the basics of plasma

physics and touring his research facility to consulting on the proper measurement techniques for gas speciation and the important measurement ranges to study.

I would like to thank my mentors during my internship with NASA Ames, Cole Kazemba, Jonathan Morgan, and Ruth Miller. I would also like to thank Dr. Alan Cassell for coordinating the internship opportunities for the HyCUBE team. My experience during the NASA Ames internship was truly invaluable, as I learned a tremendous amount about reentry modeling and the design process from them. The mentors were always willing to take the time to assist me in whatever ways they could.

I would like to thank my Akerman 30 lab-mates, Sagnik Paul, Anchal Sareen, and Yi Hui Tee for their feedback and advice throughout our weekly meetings.

I would like to thank Cooper Gray and Amy Tinklenberg (and Alice, too!) for the many, many hours spent on homework projects together. Whether we were meeting in person or over Zoom, I always enjoyed working with them (the same may not always be said about the projects, themselves).

I would like to thank Drew Schwarz, Matt Stein, and Erik Vaage for all the "lunch meetings" at Chipotle and all the physics help.

I would like to thank my parents, Phil and Kathy, for all of their unwavering love and support throughout my life and academic career. I would not be the same person I am today if they had not encouraged me to be hard-working and inquisitive from an early age. I would also like to thank my brothers, Jonathan and Joshua, for always being my competitors, collaborators, confidantes and friends.

I would like to thank my fiancée, Madison, for believing in me even when I do not believe in myself and always pushing me to be the best I can be in everything I do.

This research is supported by the Air Force Office of Scientific Research (AFOSR) under Grant No. FA9550-19-1-0308. The views and conclusions contained herein are those of the author(s) and should not be interpreted as necessarily representing the official policies or endorsements, either expressed or implied, of the AFOSR or the U.S. Government.

Thank you to the various authors and entities who gave permission for their figures to be included in this thesis.

To my fiancée,
for always getting my rear in gear.

Abstract

This thesis outlines the main design considerations of the sensor pod of a CubeSat-like, miniature re-entry vehicle, the Hypersonic Configurable Unit Ballistic Experiment (HyCUBE), that will serve as a versatile hypersonic flight test platform. HyCUBE's proposed first mission aims to collect experimental aerothermodynamic data of a hypersonic flight environment in order to investigate the chemical reactions that occur in that environment, namely the dissociation of nitrogen and oxygen. The data to be collected will contribute to the improvement and validation of computational models and ground testing methods. Numerical simulations were used to inform vehicle design decisions, using direct Simulation Monte Carlo (DSMC) method and computational fluid dynamics (CFD), when applicable and simplified estimation simulations when more appropriate. DSMC and CFD were utilized to establish the aerodynamic characteristics of the proposed vehicle, evaluate the heat-load such that the thermal protection system can be sized, and to produce three-dimensional flow solutions to guide sensor selection and placement. Simplified estimators solved the equations of motion to produce estimates for vehicle trajectories and used closed-form models to predict the aerothermodynamic environment at the vehicle stagnation point, which allowed for quick analysis of design changes. Preliminary designs for the HyCUBE vehicle form factor and sensor suite are proposed and discussed. The expected measurement environment was also used to optimize the placement of sensors to attempt maximize the amount of useful data that will be collected.

Contents

List of Tables

List of Figures

Chapter 1

Introduction

1.1 Motivation for Hypersonic Flight Testing

In order for predictive computational models for hypersonic flight to progress and improve, it is necessary that they be compared to and validated against experimental data. The data necessary for this validation can be obtained by a variety of methods that can generally be split into two categories: ground testing and flight testing. Hypersonic ground testing facilities attempt to recreate the conditions experienced in flight in a highly controlled environment. However, even with extensive knowledge in a variety of ground testing methods, there is no single ground test that can accurately recover every aspect of hypersonic flow (velocity, enthalpy, gas content, etc.) simultaneously. These shortcomings in ground testing methods give rise to the need for flight testing as the gold standard for experimental data. However, there are challenges in this sphere as well. Traditional flight testing campaigns are expensive and exclusive, reserved for only the most well-funded of researchers and engineers. In recent years, however, new technologies have emerged that promise to make gathering flight data more accessible and cost-effective. It is desirable to demonstrate the worth of these technologies, namely CubeSats, when it comes to leveraging them as research vehicles for hypersonic flow physics and flight data.

1.2 Motivation for HyCUBE

The motivation of this investigation is to develop a low-cost, efficient platform (HyCUBE) for performing scientific experiments in realistic hypersonic flight environments. Among other uses, such a flight test platform will provide a novel means to validate computational models used for hypersonic flow prediction. The relatively small platform size will also allow for joint ground and flight testing in order to provide comparative data to evaluate experimental testing methods. A key goal for the platform is to adhere to a CubeSat form-factor in order to take advantage of expanding and relatively cost-effective launch opportunities. Such launch opportunities also allow for the potential to deploy multiple vehicles in quick succession in order to obtain statistically significant data. Finally, HyCUBE can probe a regime of interest, shown in Fig. 1.1, that is difficult to reach with sounding rockets, making it a useful testing platform for reentry physics research.

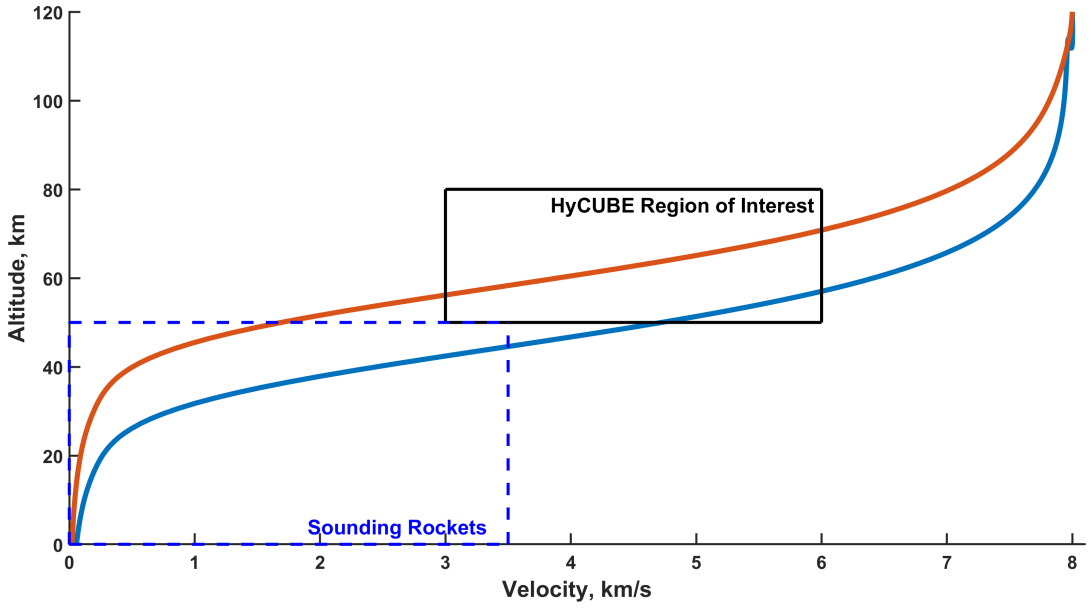

Figure 1.1: Sample trajectories for 3U (blue) and 12U (red) HyCUBE formats through the region of interest, compared to the typical operating range of sounding rocket experiments.

The HyCUBE platform is envisioned to perform experiments across a relatively broad set of conditions and flight environments achievable from orbital velocities as depicted by the sample trajectories in Fig. 1.1. It is specifically designed to be versatile allowing investigations that can vary in scope, including targeting different flow and material physics, field testing of novel sensors, and testing of experimental methodologies (e.g. transmission protocols during plasma "blackout"). HyCUBE Mark-1, will aim specifically to enhance scientific data regarding non-equilibrium chemical reaction kinetics in hypersonic boundary layers. Within the desired testing region delineated by the black box in Fig. 1.1, the flow field will fall in the continuum regime with both thermal non-equilibrium and gas-phase chemical reactions. With the motivation of generating data that can be used for validation of simulated environmental conditions, it is desirable that the flow field and boundary conditions be as simple as possible. A non-ablative thermal protection system (TPS) is therefore desirable as it will enable the modeling of a simple boundary condition as well as minimizing the presence of ablative species in the flow, allowing for easier comparisons to results from computational models post-flight. The feasibility of using such a material is a key design aspect that is considered in this thesis.

The first HyCUBE mission, HyCUBE Mark-1, will serve as a proof-of-concept mission to demonstrate that the platform is able to attain the target trajectory and conditions, and to collect and transmit the desired measurements. The entire reentry is expected to last approximately ten to fifteen minutes. The first portion of that time will be used to collect data within the region of interest, and the remainder will be spent transmitting as much of the data as possible before HyCUBE reaches Earth's surface. Data to be collected includes pressure and temperature measurements at multiple locations on the vehicle surface, gas speciation in the post-shock flow near the stagnation point, and the inertial state of the vehicle.

This thesis presents prior work on the design process of the HyCUBE Mark-1 mission concept, including scientific objectives and measurements strategies. The role of simulation in the design process is also discussed.

Chapter 2

State of the Art (Literature Review)

When it comes to collecting hypersonic aerothermodynamic data, there are two categories from which to choose: ground testing and flight testing. Each category comes with its own benefits, but also with its own limitations and challenges. In this chapter, the state of the art in each category will be explored and compared to give a sense of what conditions are achievable for measurements via each method.

2.1 Ground Testing Methods

2.1.1 Blowdown Tunnels

Blowdown tunnels are a group of ground testing facilities that use pressurized air (or other desired test gas) entering an evacuated test section through a converging-diverging nozzle to simulate low enthalpy flight conditions. The pressurized gas is heated in a staging chamber known as the plenum before entering the test section in order to avoid condensation of the gas as it expands through the nozzle [1, 2]. As the heated gas enters the test section, pressurized cold gas replaces it upstream which ensures a constant inlet condition. When the cold gas reaches the test section, the test is concluded [2]. These facilities are designed for low enthalpy flow scenarios, that is, flow temperatures below

2000 K and/or velocities less than 2 km/s. In this regime, the ideal gas law holds and thus the Mach-Reynolds-simulation method applies [2]. This method takes advantage of the fact that at low speeds, the flow properties only depend on dimensionless quantities such as the Mach and Reynolds numbers and therefore sub-scale models can be used to predict the behavior of the flow around the full-scale vehicle.

Blowdown tunnels are capable of achieving long test times, on the order of seconds to minutes, but the conditions they can reach are limited. The simulated velocities and total temperatures replicated by blowdown tunnels are often not sufficient for many hypersonic investigations. Typically, the total temperature achievable with a blowdown tunnel is under 2000 K which corresponds to an equivalent velocity of only 1.5 km/s at sea level conditions [2]. The limited enthalpy at which these tunnels operate also excludes them from being able to investigate chemical effects of the flow [1]. A further potential limitation is that for tunnels with fixed pressure reservoir volumes, flow properties will vary as the test is operating, with velocity, for example, decreasing with time as the pressure differential begins to equilibrate [2].

2.1.2 Shock Tunnels

Shock tunnels are a group of ground testing facilities that rely on a shock wave traveling through a test section to produce higher enthalpy flows than are possible in blowdown tunnels. Reflected shock tunnels create a shock wave upstream of a converging-diverging nozzle using a heated, pressurized driver gas to propel the desired test gas. The test gas becomes stagnated in the converging-diverging nozzle before undergoing unsteady expansion into the test section [2]. This results in a high enthalpy testing environment, with flow exceeding 2 km/s velocity and 2000 K temperature. The test is considered to be complete when the driver gas reaches the test section.

While shock tunnels are able to achieve higher enthalpy flow conditions, their test times are very short, on the order of milliseconds or even microseconds [2]. This is typically long enough to capture the gas chemistry effects, but still there is a lack of ability to perform extended tests to fully simulate a flight. These short testing times are caused by three inherent aspects of shock tunnels: wave reflection of driver-test gas

interface, shock-boundary interaction with nozzle inlet, and precursor shock damping downstream of the test section. A shock reflection off of the interface between the driver gas and the test gas can alter the aerothermal properties of some regions of the flow and can therefore shorten the amount of testing time with optimal conditions. The interaction of the shock with the nozzle can cause the test gas to stagnate in the nozzle inlet while still allowing the driver gas to flow around this stagnated gas in the boundary layer, resulting in early driver gas contamination and shortening the testing time. Finally, the moving shock can reflect off the back of the vacuum tank and move back through the test section, altering the flow conditions. These challenges and potential solutions in order to increase test times are explored in [1].

2.1.3 Arc-Jets

Arcjet facilities provide a way to accurately recreate the heat flux experience in-flight by subjecting a test subject to super heated exhaust flows of a test gas. These facilities are capable of producing high enthalpy flows that accurately simulate the heat flux experienced in flight, up to 2500 W/cm^2 [3]. These capabilities are extremely useful for investigating thermal protection system (TPS) performance and can be used to measure surface recession and ablation and the in-depth temperatures of the material [4].

The limitation of arcjet facilities, however, is that they are largely unable to recreate the flow physics and chemistry experienced in flight. They are able to replicate the enthalpies and heat fluxes required, but not the free-stream conditions of the flow and thus are unhelpful at determining the flow's aerodynamic environment [4]. These facilities can achieve limited pressure and mass flow levels due to the large volume of gas needed to be heated by the arc to create such conditions. The flow is also often contaminated with combustion products such as H_2O and CO_2, which are not realistic for in-flight conditions [1].

2.2 Flight Testing Methods

2.2.1 Heritage Missions

The first data from hypersonic reentry vehicles were obtained in the mid-20$^{\text{th}}$ century during the early days of space exploration using reentering orbital capsules. During the Mercury program, a to-scale prototype vehicle, nicknamed Big Joe, was flown to assess the performance of the proposed TPS material. The Big Joe vehicle entered from orbit at a speed of 6.4 km/s at an altitude of approximately 110 km and maintained high speeds throughout its reentry, as at approximately 30 km altitude its speed still exceeded 3 km/s [5]. The vehicle contained 104 thermocouples, half in the forebody heat shield and half in the afterbody, 13 char sensors, and two pressure sensors [6]. These sensors provided insight into the heating of the craft and identified a location of high heat flux on one side of the vehicle afterbody, which had not been predicted in pre-flight design and ground testing. This was determined to be an area of transition from laminar flow to turbulence when the separation layer reattached behind the forebody and prompted a change of TPS in that region for subsequent Mercury flights [5, 6]. The Mercury program's successor, the Gemini program, also provided similar hypersonic flight data that is discussed in [5, 6].

The Fire Program consisted of two unmanned capsule flights, serving as proof-of-concept precursors for the manned Apollo missions, that assessed the reentry environment. FIRE-I encountered stability issues and as a result much of the data is not useful or hard to interpret [6]. FIRE-II, however, offers a wealth of useful data. The FIRE-II spherical forebody was heavily instrumented in three layers of beryllium that could be detached at certain points during reentry to expose the subsequent sensor layers to the incoming flow. The vehicle forebody instrumentation included three radiometers (one spectral radiometer and two total radiometers) and 114 thermocouples. The afterbody instrumentation added an additional 12 thermocouples, an additional total radiometer, and a static pressure port [7]. This large amount of instrumentation provided a wealth of aerothermodynamic data that is still useful decades after its launch. Computational fluid dynamics (CFD) analysis was performed on the FIRE-II flight and compared to

flight data, which showed good agreement, within the range of the experimental uncertainty when the correct boundary conditions were applied. However, if simpler boundary condition models were used, the heating could be overestimated or underestimated [6]. This CFD comparison underscores the need for flight data to evaluate and guide the development of computer models.

During the Apollo program, four unmanned flights were performed focused on improving the understanding of the heating environment upon lunar reentry. The first two, AS-201 and AS-202, reentered at orbital velocities, while the subsequent Apollo 4 and Apollo 6 achieved super-orbital velocities by introducing a kick stage to better replicate lunar reentry [6]. AS-201 and As-202 investigated the heating rate and the heat load of the proposed TPS, respectively. Both vehicles were equipped with 12 calorimeters and 12 pressure sensors on the forebody heat shield and an additional 23 calorimeters and 24 pressure sensors on the afterbody [7]. Unfortunately, heating data from the forebody was lost on both flights due to sensor failures during reentry. However, some pressure data and afterbody heating data did survive [5–7]. This surviving data allowed for comparison with pre-flight wind tunnel testing and with modern CFD analysis. Apollo 4 and 6 expanded on their predecessors by reentering at superorbital velocity, with Apollo 4 reentering at over 11 km/s and Apollo 6 reentering at approximately 10 km/s [5]. These missions focused on demonstrating the readiness of the Apollo flight technology, which included collecting aerothermal data. These flights were equipped with 17 pressure transducers, four radiometers, and 32 calorimeters, redesigned to avoid the failures of AS-201 and AS-202 [7]. The flight test data agreed well with predicted values for the forebody section of the vehicle, but the pressure and heating readings on the afterbody were around 1/3 to 1/2 the expected values, possibly due to the presence of more ablation products in the flow than were expected because of the unprecedented velocities [5, 6].

More recent examples of large-scale reentry missions include the MIRKA and ARD capsules. MIRKA (Micro Reentry Capsule) was a spherical capsule with a flat base that used a Russian FOTON rocket to deliver it to orbit. The vehicle achieved reentry speeds of 7.6 km/s and measured the flow using two pyrometers, three rarefied flow

pressure sensors and 25 thermocouples. The TPS was SPA (surface-protected ablator) coated with silicon-carbide [6]. ARD (Atmospheric Reentry Demonstrator) featured a more traditional capsule design with a spherical forebody and a conical afterbody. ARD reentered at speeds of 7.5 km/s carrying seven pressure transducers, 14 thermocouple plugs, plus an additional two plugs on the back shell, surface pressure sensors and surface mounted calorimeters. The forebody TPS material was an ablative tile made of silica and phenolic resin [6, 8].

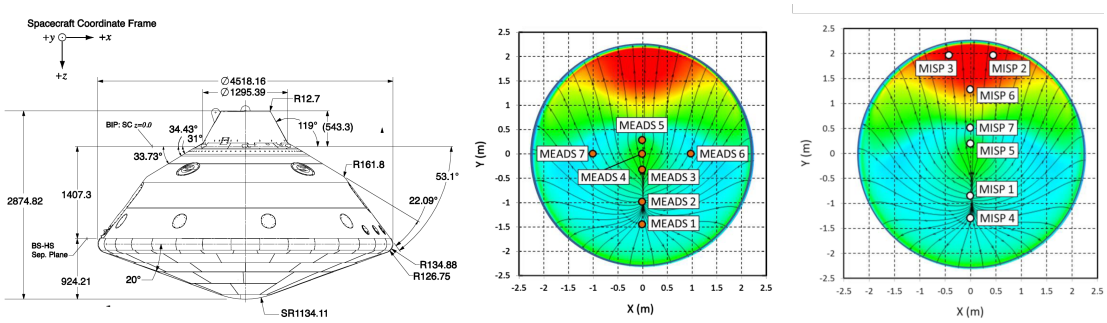

Figure 2.1: The configuration of the MSL capsule and locations of the MEDLI pressure ports and MISP plugs. Adapted from Reference [9].

The Mars Science Laboratory (MSL) was a capsule-like vehicle designed to deliver the Curiosity rover to the surface of Mars. During its entry phase, many aerothermodynamic properties of the Martian atmosphere were collected using the MEDLI (MSL Entry, Descent, and Landing Instrumentation) sensor suite. The vehicle measured pressure using MEADS (Mars Entry Atmospheric Data System), a collection of seven pressure ports distributed in a cross-like formation (as shown in Fig. 2.1) around the capsule's forebody at locations where the flow would remain laminar to avoid high heating rates. Some ports were placed near the stagnation point to measure stagnation pressure, while others were placed downstream on the pitch plane or on opposite sides of the pitch plane to detect angle of attack and slip angle, respectively. The MEADS system measured pressures between 0-34 kPa and was sampled at 8 Hz. In addition to the determination of flight angles, the pressure data collected also was valuable in validation of modeling efforts for entry into the Mars atmosphere [9, 10]. Temperature and heat flux for the

mission were measured using seven MISP (MEDLI Integrated Sensor Plugs) plugs embedded in the ablative PICA tiles of the forebody TPS. Each plug contained four type K thermocouples at known depths in the TPS material, and an isotherm sensor. The thermocouples near the surface measured the surface heating, while the deeper thermocouples measured the ablative TPS tiles' in-depth response. The isotherm sensor measured the progression of the char layer as the tiles ablated. The MISP plugs were arranged along or near the line of symmetry (also shown in Fig. 2.1) of the vehicle in order to observe the growth of the boundary layer and to investigate the region of transition from laminar to turbulent flow [9]. A follow-up mission to MSL, the Mars 2020 mission, also used a similar vehicle design with similar instrumentation, the MEDLI2 sensor suite. The arrangement of MEDLI2 sensors was adjusted using data from MSL (MEDLI) flight data, with an increased focus on collecting afterbody aerothermal data [11].

Large-scale missions like those discussed in this section have provided valuable hypersonic flight data for investigation of TPS performance, laminar to turbulence transition, and general characterization of hypersonic flow environments. This type of mission, however, is an extremely expensive option to collect flight data, and thus there are few groups with sufficient funding to produce such a mission. This high cost also limits the number of flights a certain mission or program is able to produce, and makes it difficult to make design adjustments and repeat a given test. As hypersonic technology has advanced, lower cost options for flight testing have emerged to attempt to fill this role which will be discussed in the following sections.

2.2.2 Sounding Rockets

In the 1950s and 1960s, sounding rockets were introduced as an alternative to large-scale reentry missions as a relatively low-cost means to collect in-flight experimental data. Sounding rockets are capable of carrying scientific and engineering payloads to investigate hypersonic flow phenomena, for instance laminar to turbulent transition and thermal protection system performance.

The Bow-Shock UltraViolet (BSUV) experiments were a series of two sounding

rocket flights that studied the gas emission of flow behind the bow shock of a blunted sounding rocket nose tip with a 10 cm nose radius. The rockets achieved measurement conditions of 3.5 km/s during ascent from 40 to 70 km altitude (on Flight 1) and 5 km/s during the descent from 110 to 65 km altitude (on Flight 2). The gas was measured using UV scanning spectrometers, probing the frequency range of 200 to 400 nm, and radiometers, which were calibrated to specific emission bands of the species of interest. One spectrometer was pointed directly out of the nose tip, while the radiometers were placed on the side of the nose, downstream from the stagnation point [12, 13]. The main species of interest was NO, which forms through a two-step process through dissociation of nitrogen and oxygen molecules and their combination. The concentration of NO was measured and its variation with altitude was assessed. It was found that the concentration of NO agreed well with predictions for lower altitudes, below 80 km. At higher altitudes, however, the models significantly underestimated the emission of the gamma band of NO. [13–16]. It was also observed in these flights that there was a strong OH emission from dissociated water molecules. This band was also evaluated for altitude dependence [12–14]. The data from the two flights were used to create improved models for chemically reacting hypersonic flows. The issue of underestimating NO emission at higher altitudes led to an improved model for oxygen dissociation for both high altitude CFD and DSMC methods [12, 16–18].

The HIFiRE (Hypersonic International Flight Research Experimentation) program from the Air Force Research Labs is a series of sounding rockets dedicated to the collection of hypersonic aerothermodynamic data. The program focused on filling in gaps in existing hypersonic data and especially on areas that were unable to be modeled with ground testing methods. HIFiRE-5 featured an elliptical cone nose with a 2:1 aspect ratio, a minor axis half-angle of 7.5 degrees, and a nose tip radius of 2.5 mm [19] (previous HIFiRE iterations featured a circular cone nose [20]). The HIFiRE-5 nose was heavily instrumented with thermocouples, embedded in the steel and aluminum portions of the heat shield, and six Schmidt-Boelter type heat flux sensors. The nose instrumentation also included three models of pressure transducers - low frequency static pressure gauges, six high frequency gauges to detect pressure fluctuations, and four differential

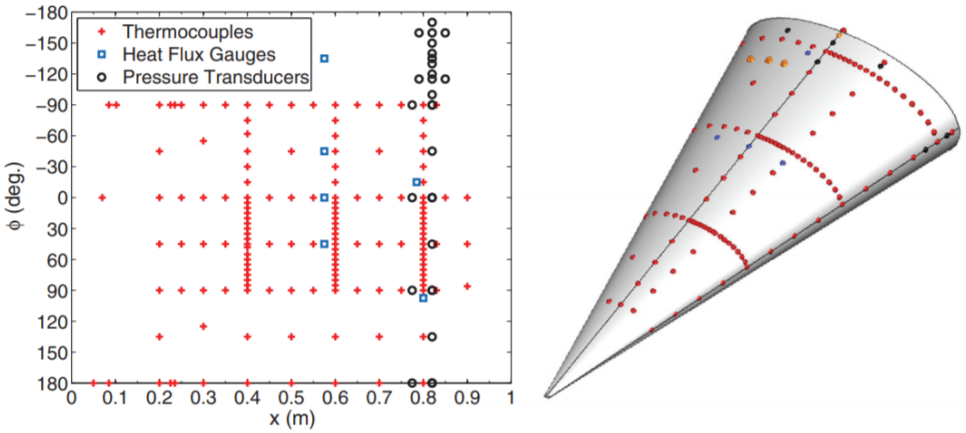

Figure 2.2: The sensor arrangement of the HIFiRE-5 sounding rocket experiment on its elliptical cone nose. Republished from Reference [19].

pressure gauges to aid in attitude determination. The sensor arrangement of HIFiRE-5 can be seen in Fig. 2.2. The sensor data collected by HIFiRE-5 was used to investigate the boundary layer transition along its conical nose [19].

The upcoming Boundary Layer Transition (BOLT) experiment from Johns Hopkins University Applied Physics Laboratory is another sounding rocket experiment that aims to provide flight data to improve the predictive capabilities of CFD models, with a specific emphasis on the prediction of boundary layer transition from laminar to turbulent. The BOLT rocket carries a uniquely shaped nose tip that features four swept leading edges, and two concave surfaces separated by concave "gutters." The nose is made of made of iridium-coated titanium–zirconium–molybdenum (TZM) at the tip, which is followed by a section of stainless steel and then a section of aluminum. The experiment aims to induce a transitional region on the two symmetric concave surfaces that can then be measured and studied. This experiment will be conducted during both the ascent and descent portions of the trajectory. During ascent, the test will be conducted at altitudes from 13 to 38 km, reaching 1.4 to 1.8 km/s. During descent, the experiment will last from about 40 km until about 18 km altitude, reaching approximately 2.0 to 2.2 km/s. In order to capture aerothermodynamic data, BOLT will carry over 300 sensors at over 200 discrete locations on the nose tip. The majority of the sensors will

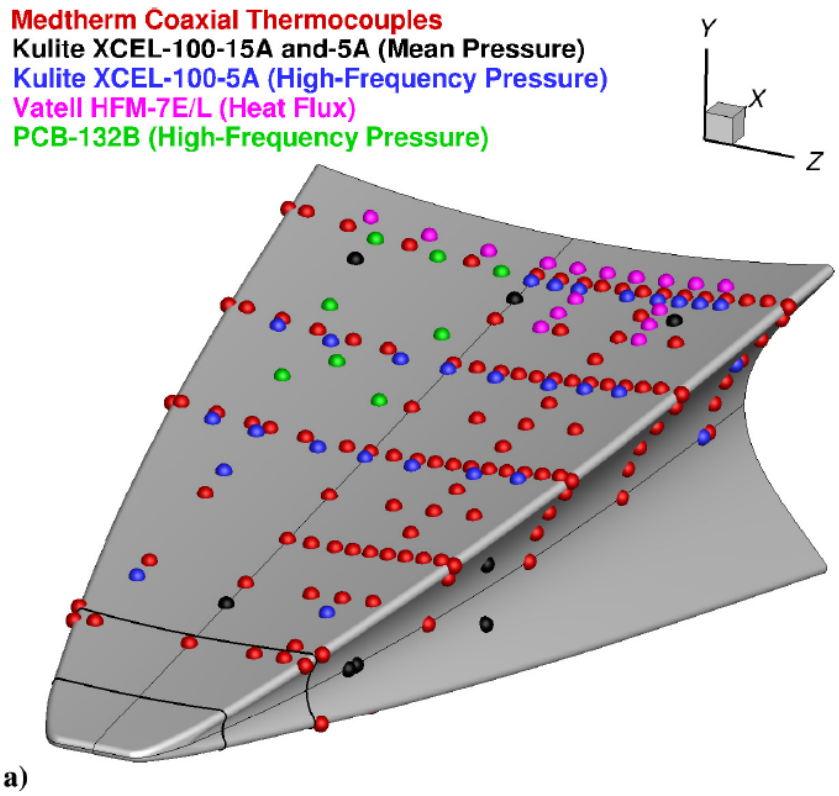

Figure 2.3: The sensor arrangement of the BOLT sounding rocket experiment nose tip. Republished with permission from the American Institute of Aeronautics and Astronautics (AIAA), from Reference [21].

be thermocouples, but other sensors include two varieties of pressure transducers – one for static pressure and one for pressure fluctuations – and a heat flux sensor [21]. The arrangement of the various sensors can be seen in 2.3.

TPS demonstration is a common focus of sounding rocket missions, as well. The SHARP (Slender Hypervelocity Aerothermodynamic Research Probes) program of sounding rockets aimed to demonstrate the usefulness and feasibility of UHTC (Ultra High Temperature Ceramic) TPS materials. SHARP-B2 flew four strakes outfitted with this TPS material protruding from the sharp, conical nose [23]. Similarly, DLR's SHEFEX (Sharp Edge Flight Experiment) program of sounding rockets also investigated the performance of a novel, sharp-edged TPS made of carbon-carbon silicon carbide

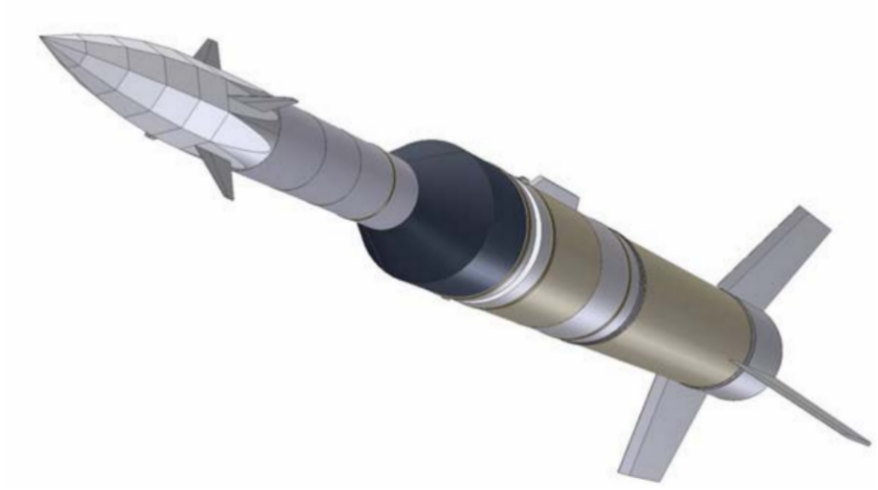

Figure 2.4: The SHEFEX sounding rocket configuration. Republished with permission from DLR MORABA, from Reference [22].

tiles. It also demonstrated the use of a novel aerothermal data collection system. The SHEFEX-II rocket features a pointed nose tip that is covered with the TPS tiles and heavily instrumented with sensors for pressure, temperature and heat flux. The SHEFEX configuration and the sharp, tiled nose can be seen in Fig. 2.4. The rocket's apogee was approximately 180 km, where it reached velocities of around 2.3 km/s. The maximum velocity reached was almost 2.8 km/s at around 30 km altitude during the descent phase. Aerothermodynamic data was collected during both the ascent and descent phased of the rocket's trajectory. Three select points along its trajectory during the ascent phase were compared to CFD analysis and show very good agreement [22, 24].

Sounding rockets have provided a tremendous amount of value to hypersonic flight testing, having been used to investigate bow shock radiation, laminar to turbulent transition, and TPS performance. However, these sub-orbital rocket flights are typically limited to lower velocities and are not able to produce the types of conditions that are possible with orbital reentry flights. Also, while they are a lower cost option than the large-scale flights discussed in section 2.2.1, they are still quite expensive. The following sections discuss low-cost orbital flight options.

2.2.3 CubeSat Reentry Vehicles

In recent years, there has been an increase in missions aimed at using small-scale reentry vehicles to obtain hypersonic flight data. One option for these flight tests are CubeSats. CubeSats are a class of small satellites that comply to a strict set of requirements, like size and weight, which enable cost-efficient manufacturing and launch opportunities. These satellites can be made in sizes measured in increments of the standard CubeSat unit (U). 1U is a 10 cm $\times$ 10 cm $\times$ 10 cm cube that weighs between 1 and 1.33 kg [25]. These requirements allow for many standardized CubeSat components to be easily obtained off-the-shelf and for many standardized launch methods to be developed and used at relatively low costs.

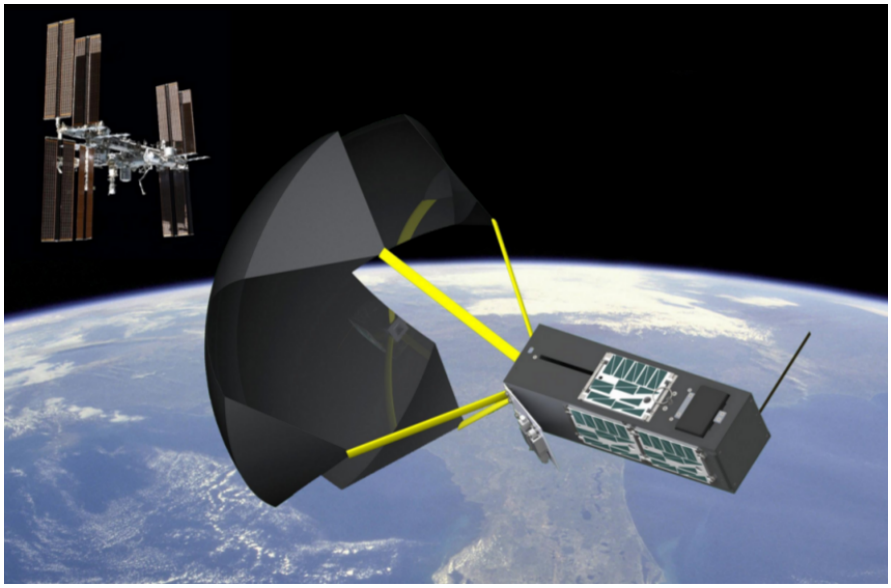

Figure 2.5: Concept image of TechEdSat-4 featuring the ExoBrake drag sail. Republished from Reference [26].

The longest-running program using CubeSat reentry vehicles is the TechEdSat program at NASA Ames Research Center, which has launched more than ten CubeSat vehicles. In 2012, TechEdSat-1 was the first CubeSat to be launched from the International Space Station [27]. TechEdSat is now a series of satellites that has performed both scientific and engineering-oriented test flights. The first two TechEdSats were

1U proof-of concept flights that tested ejection methods and communication systems. TechEdSat-3 increased the vehicle size to 3U and also introduced a novel drag deorbit device, the ExoBrake. This device, shown deployed behind TechEdSat-4 in Fig. 2.5, was further tested in subsequent missions [28]. For instance, TechEdSat-5 tested modulation strategies of the ExoBrake to improve active control, and TechEdSat-8 pushed the temperature limits of a modified 'hot' ExoBrake to evaluate its performance at lower altitudes [29]. Through its almost ten CubeSat flights, the TechEdSat program has demonstrated that CubeSat reentry flights are a viable means to produce hypersonic flow conditions and can be done so while maintaining vehicle stability. Further, the program has shown that CubeSat vehicle are able to survive deep into the atmosphere and it is feasible to transmit collected data from the vehicle to the ground station even until these lower altitudes.

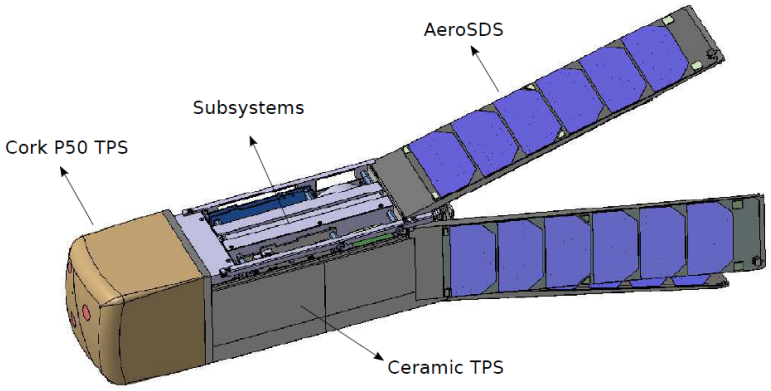

Figure 2.6: The QARMAN CubeSat vehicle. Republished from Reference [30].

The von Karman Institute's QARMAN (shown in Fig. 2.6) is another reentry vehicle that utilizes CubeSat technology to collect hypersonic flight data. QARMAN (Qubesat for Aero-thermodynamic Research and Measurements on AblatioN) is a 3U CubeSat with a blunt leading edge made of an ablative thermal protective material, cork P50. In addition to this forebody thermal protection, the vehicle also is protected by silicon carbide-coated titanium along its sides. A key focus of the mission was to assess the performance of these thermal protection systems [31]. QARMAN carries on board three

thermocouple plugs embedded in the cork TPS, three pressure sensors, and an emission spectrometer. The thermocouple plugs and pressure taps are even spaced in three of the four quadrants of the nose, with the thermocouple plugs closer to the geometric center of the nose for the the on-diagonal group of sensors, but the pressure tap closer to the geometric center of the nose for the off-diagonal group of sensors. The spectrometer viewing port is placed at the geometric center of the nose, pointing directly forward out of the nose [30, 32]. QARMAN was launched in 2020 and is currently on-orbit.

This area is also the subject of student-level research. For example, SASSI^2 is a joint project between the Purdue University and the University of Illinois. This CubeSat reentry vehicle will serve as a platform to collect aerothermodynamic data as well as information on the chemical species present in the flow. SASSI^2 will carry sensors to measure pressure, heat flux and the gas species, focusing on the low-density region of the atmosphere between 100 to 200 km altitude [33, 34]. This data will help validate direct simulation Monte-Carlo (DSMC) models that are used instead of traditional CFD at these altitudes. SASSI^2 is still in the development stage.

CubeSats promise to be a low-cost means to provide hypersonic flight data for a variety of conditions. The amount of launch opportunities and low cost of development hold the potential for customizable, repeatable tests that will allow for investigations for a variety of scientific objectives. The information available to date from these missions is largely related to technology demonstration. It has been shown that CubeSat reentry vehicles can probe hypersonic conditions and collect hypersonic measurements into the beginning of the continuum regime, as evidenced by the TechEdSat series. Other important technology that has been demonstrated is the use of drag deorbit devices for controlled reentry. Also, the use of radio communication systems like Iridium and GlobalStar has been demonstrated as a reliable means for data transmission. In this early stage of CubeSat development, however, there is not any publicly available aerothermal data from a CubeSat reentry mission.

2.2.4 Small Reentry Capsules

Reentry capsules are another option for small-scale flight tests. These capsules commonly feature a blunted cone forebody and a spherical afterbody, surrounded by thermal protection material. Capsules are commonly designed to fit inside a CubeSat form factor so they can take advantage of CubeSat launch opportunities.

The Aerospace Corporation's Reentry Breakup Recorder, or REBR, is a small-form reentry capsule that was designed to investigate the breakup of reentry vehicles as they burn up in the atmosphere in order to assess and improve computer models that predict a vehicle's survivability. The REBR capsule is designed to piggyback onto a host vehicle and as the host reenters the atmosphere, the capsule detaches to perform the experiment. The capsule, contrary to the heritage mission capsules, features a blunted cone forebody and a spherical afterbody, which, with appropriate placement of the center of gravity, makes it self-stabilizing across all flight regimes. REBR was outfitted with a sensor suite consisting of two IMUs, and up to eight thermocouples. Internal temperature and pressure were also measured by the on-board computer [35, 36]. REBR's self-stabilizing design has been an attractive design choice for various other reentry capsules as well and has inspired tag-along missions, for example the RED program, the MIRKA2 capsule and the KRUPS vehicles. The RED (Reentry Device) program is a commercial equivalent to REBR and features several models all aimed at investigating the breakup of vehicles and debris upon reentry [37]. The MIRKA2 (Micro Reentry Vehicle 2) capsule features an identical design to REBR but scaled down so it fits into a 1U CubeSat form factor. The vehicle carries six in-depth thermocouples, two dynamic pressure transducers, and a cyanide radiometer which will evaluate the ablation of the vehicle TPS, which is RICA. There is also an IMU and GPS on board to track the vehicle's inertial state and position [38]. Another similar mission to REBR is SPRITE (Small Probe Reentry Investigation for TPS Engineering). While featuring a similar design to REBR, it is not clear if it was inspired by REBR or independently developed. SPRITE aims at demonstrating TPS material performance while incorporating NASA's "test like you fly" policy, in which the same vehicle is used in ground tests and flight tests [39].

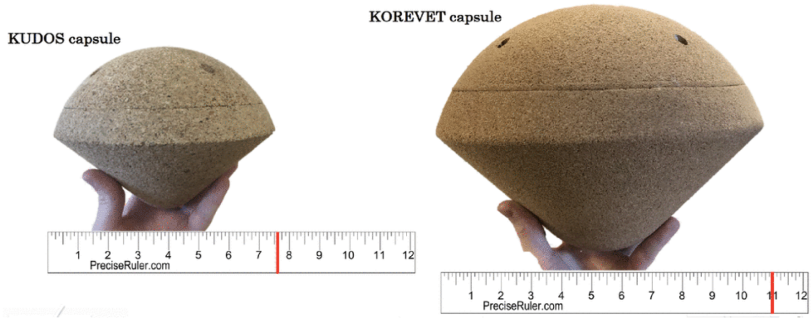

Figure 2.7: The sub-orbital KRUPS capsules, KUDOS and KOREVET. Republished with the permission of the author from Reference [40].

The KRUPS program at the University of Kentucky is another of several mission series that take inspiration from the REBR capsule. The KRUPS vehicles utilize the same self-stabilizing capsule design as REBR. The first three KRUPS flights, KUDOS and KOREVET I and II, performed sub-orbital flights using sounding rockets as a payload delivery mechanism. These sub-orbital missions were aimed at demonstrating the technology readiness of the KRUPS technology including validating the ejection method from the rocket housing and the testing the communication systems. These capsules utilized a hardened cork ablative TPS instrumented with three embedded thermocouple plugs [40, 41]. Unfortunately, various issues in communication systems and ejection methods prevented the three sub-orbital flights from collecting and/or transmitting meaningful data [40–42]. A fourth KRUPS flight initiative, called KREPE, is a series of three capsules slated to launch in July 2021. These flights will be the first orbital flights of the program. The goals of KREPE are to provide a testbed for TPS evaluation and to collect aerothermal data to validate predictive computational models. The KREPE capsules also utilize the REBR-inspired form factor, but use a more robust TPS material than the cork used in the sub-orbital flights. Two of the KREPE capsules will use LI-2200 shuttle tile coated reaction cured glass (RCG) and the third will use a novel 3D-printed TPS material. High-density cork will still be used to insulate the afterbody as it will not experience the levels of heating that the forebody will. Each capsule will measure heating using surface-mounted thermocouples, as opposed to the thermal plugs

used in the sub-orbital flights [42].

Small-scale reentry capsules, like CubeSats, have potential for low-cost hypersonic flight collection. There is more data available in this category than there is for CubeSat missions, mostly investigating the heating environments of reentry vehicles and TPS material performance. With the onset of CubeSat launch opportunities, capsule missions like KRUPS have been able to take advantage as well by designing adapters to make the vehicles compatible with launchers.

Chapter 3

HyCUBE Objectives

3.1 Scientific Goals

The first HyCUBE flight, HyCUBE Mark-1, will aim to improve understanding of chemical reaction rates and molecular relaxation rates in a nonequilibrium hypersonic flow environment. The vehicle will collect time series aerothermodynamic quantities and gas species emission within the desired regime of interest. This experimental data will be useful for comparison with state of the art models of reaction rates and relaxation rates in hypersonic flow. Through this comparison, these models can be assessed and potentially improved.

3.2 Targeted Flight Conditions

The desired flight regime of the HyCUBE Mark-1 mission is a high Mach number, non-equilibrium flow in the continuum regime with gas dissociation (while avoiding strong ionization). To conform with this regime, the vehicle must reach velocities of 3 km/s to 6 km/s within the altitude range of 50 km to 80 km. This region is depicted by the black box in Fig. 1.1. Achieving the lower bounds of these conditions will ensure high Mach number, non-equilibrium flow with the desired gas dissociation effects. The upper bounds guarantee that the flow will be in the continuum regime while avoiding strong

ionization effects. The gas composition is expected to be dominated by the five species that are a result of gas-phase chemistry of molecular nitrogen and oxygen: N_2, O_2, N, O, and NO. While gas ionization is expected at high entry speeds, the presence of ionic species increases complexity of the reacting gas system, and further complicates data analysis for inferring the nonequilibrium chemical kinetics. Thus it is desirable that the re-entry trajectory be such that ionic species are nonexistent, or that their presence is minimized to the largest extent possible.

3.3 Proposed Mission and Vehicle Concept

In order to study the flow field at the desired conditions, HyCUBE Mark-1 will carry multiple pressure transducers and thermocouples, a spectrometer and an inertial measurement unit (IMU). Pressure will be measured near the stagnation point as well as at additional stream-wise locations *along* the body for several circumferential positions *around* the body. Temperature will be measured at similar locations at specific depths according to the chosen thermal protection material, which will allow the calculation of local heat flux. Gas speciation will be observed along a line of sight facing outward near the nose. The IMU will be used to determine the vehicle's inertial state, including its velocity, angle of attack, roll angle, and rate of spin. It is expected that all data will be used in tandem to infer the precise flight environment.

Placement of the sensors will be guided by modeling and numerical simulation. This is such that final placement of sensors will result in maximum information content to support the scientific objectives. Additionally, simulation results will guide the choices of the data acquisition rates required to observe the vehicle dynamics, heat-loading history, and evolution of aerothermodynamic quantities during re-entry.

Two possible vehicle designs have been analyzed and are presented here. The original form factor considered was a 3U CubeSat-like cylindrical vehicle with a hemispherical nose of radius 5 cm, as shown in Fig. 3.1a. Note that a 'U' is the standard CubeSat unit, measuring 10 cm $\times$ 10 cm $\times$ 10 cm. The majority of the work presented in this thesis is based on this design. However, simulation results (presented in detail in section 4.3)

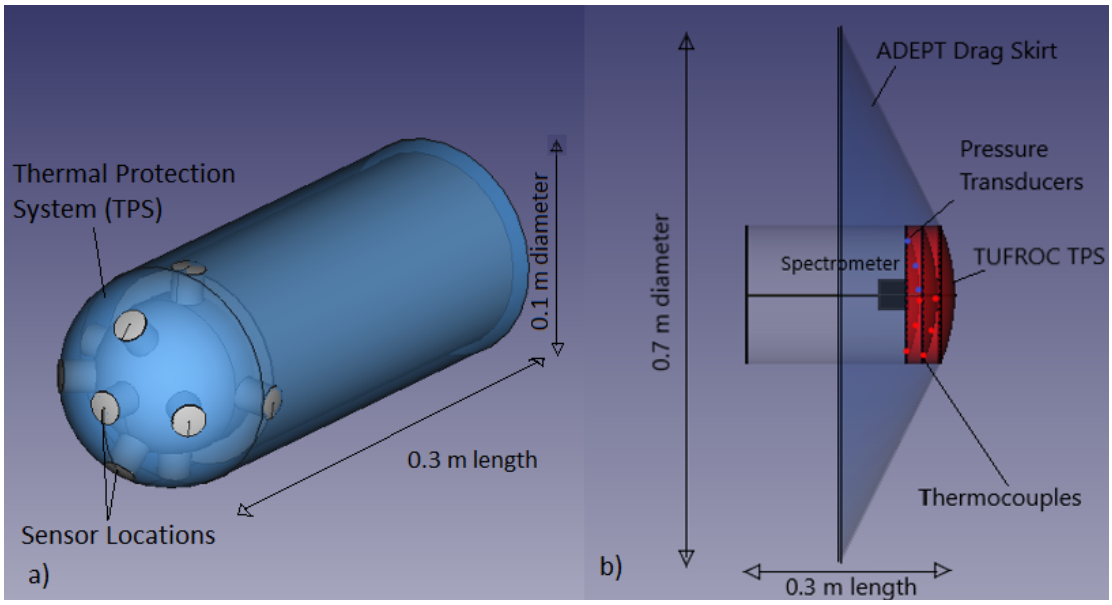

Figure 3.1: The a) original 3U and b) modified 12U HyCUBE sensor pod concept.

have indicated that this design may not be viable without the use of an ablative thermal protection system, forcing a redesigned form factor to be considered if a non-ablative material is to be used. That redesign, shown in Fig. 3.1b, includes a larger CubeSat body, an increased nose radius and a drag skirt extension, inspired by the ADEPT SR-1 [43]. The redesigned vehicle features a 2U $\times$ 2U $\times$ 3U CubeSat format with a 25 cm radius nose. The drag skirt acts to further increase drag on the body and hence decrease the vehicle speed. This work focuses primarily on analysis of the original 3U concept. In the future, similar analysis will be completed on the redesigned vehicle and on any competing design.

A key parameter that is central to the HyCUBE's first mission design is the ballistic coefficient, defined as:

$$B = \frac{m}{A \cdot C_{\mathrm{D}}} \tag{3.1}$$

where m is the mass of the vehicle, A is the frontal area, by convention, and C_D is the drag coefficient along the body axis of the vehicle, also by convention. Representative values of the ballistic coefficient were calculated for the two HyCUBE vehicle designs

for use in engineering-level design decisions, using Eq. 3.1. An important assumption in these calculations was that the ballistic coefficient was constant throughout the entire flight, when in reality it varies as the drag coefficient decreases with altitude, and also as pitch and roll of the vehicle alters the effective front-facing area. Thus, the fixed ballistic coefficients were used to calculate *approximate* vehicle trajectories; it was found that this assumption is adequate for the purpose of this investigation.

The mass of a 3U CubeSat is assumed to be 4 kg, and the vehicle is cylindrical with a radius of 5 cm, giving a cross-sectional area of 7.85×10^{-3} m. The drag coefficient in the "orbital decay phase" was estimated to be about 2.5, based on CFD analysis that was ongoing at the time. These calculations gave the ballistic coefficient for the 3U concept to be approximately 200 kg/m^2. For the 12U concept, the calculation was reversed to find the vehicle parameters needed to ensure a ballistic coefficient of 30 kg/m^2. Using flight data from the ADEPT-SR1, the drag coefficient of the vehicle with the ADEPT drag skirt vehicle was inferred to be 1.44. Extrapolating the CubeSat vehicle mass to account for the increased in size to 12U and adding the weight of ADEPT, the mass was assumed to be 16 kg. Finally, the cross-sectional area of the drag skirt was calculated to be 0.38 m^2, which gives a skirt diameter of 70 cm. These design parameters produce the desired ballistic coefficient value of 30 kg/m^2.

Throughout the design process, dynamic stability of the vehicle, data transmission, and system integration must also be considered and work is ongoing in these areas [44].

Chapter 4

Expected Measurement Environment

The design process of the HyCUBE sensor pod is driven by the top-level constraints: achieving the conditions in the regime of interest and maintaining a flowfield free of ablation products while adhering to a CubeSat footprint and standards. The vehicle will follow a ballistic trajectory during its reentry, assuming no active attitude control on-board. Therefore, the reentry trajectory is affected only by the initial conditions (namely entry altitude, entry velocity and entry flight path angle) and the vehicle's ballistic coefficient. It is currently assumed that the vehicle will be launched from the International Space Station (ISS) and thus will begin its reentry phase from an approximately circular orbit at about 400 km altitude. The remaining parameter we have control over to ensure the vehicle achieves the conditions of regime of interest is the ballistic coefficient, B (Eq. (3.1)).

In order to evaluate the vehicle's trajectory and the expected conditions through the reentry, both full-accuracy and simplified numerical models were used. High-fidelity computational models (both CFD and DSMC) were used to determine the aerodynamic coefficients of the vehicle at a variety of altitudes, velocities and angles of attack. These methods were also used to obtain three-dimensional solutions of the flow field conditions *surrounding* and surface conditions *on* the vehicle. While these high-fidelity numerical

methods are more accurate and yield comprehensive results, they are not always necessary for testing and directing various design choices. To expedite some of the design decisions, a simple tool was built using closed-form expressions to evaluate the vehicle trajectory and expected stagnation point conditions for a range of input parameters, when appropriate.

4.1 Stagnation Point Conditions: An Estimation Tool

4.1.1 Trajectory via the Allen-Eggers Method and the Full Equations of Motion

The trajectory of a ballistic reentry vehicle is governed by the planar equations of motion, which can be written in parametric form as shown in Eqs. 4.1, 4.2 and 4.3 [45]. Here, the time rate of change of the state variables y, V, and γ (altitude, velocity, and flight path angle) are described based on planetary atmosphere properties and vehicle properties. The planetary properties are ρ_0, a reference atmospheric density chosen to be density at sea level, β, the inverse scale height, g, acceleration due to gravity, and R_0, a reference distance from the planet's center chosen to be the planetary radius at sea level (i.e. an altitude of 0 km). The values for the planetary properties are given in Table 4.1. The vehicle properties are B, the ballistic coefficient (assumed to be a constant), and $\frac{L}{D}$, the ratio of the lift and drag coefficients. Note that the lift-to-drag ratio for a ballistic trajectory is zero.

$$\frac{dy}{dt} = V\sin(\gamma) \tag{4.1}$$

$$\frac{dV}{dt} = -\Big[\frac{\rho_0}{2B}\exp^{-\beta y}\Big]V^2 + g\sin(\gamma) \tag{4.2}$$

$$\frac{d\gamma}{dt} = -\Big[\frac{\rho_0}{2B}\exp^{-\beta y}\Big]V\Big(\frac{L}{D}\Big) + \frac{g}{V}\cos(\gamma) - \frac{V}{R_0+y}\cos(\gamma) \tag{4.3}$$

This set of equations is highly non-linear, which makes finding an analytic solution

Property	Symbol	Unit	Value
Reference Density	ρ_0	m/kg^3	1.226
Inverse Scale Height	β	1/m	1.378×10^{-4}
Gravitational Acceleration	g	m/s^2	9.81
Planetary Radius	R_0	m	6.378×10^6

Table 4.1: Planetary properties used in trajectory simulations [46].

impossible in their current form. They can, however, be simplified through the use of clever assumptions and, as was found by Allen and Eggers, a closed-form solution may be obtained [47]. The key assumption made during the derivation by Allen and Eggers is that the gravitational force is negligible compared to the drag force for sufficiently steep entry angles. Other assumptions include that the flight path angle is constant, that density varies exponentially with altitude, and that the reentry follows a ballistic trajectory. These assumptions allow the reduction of the equations of motion to the Allen-Eggers equation, given in Eq. 4.4, which gives the velocity at a certain altitude when provided an entry velocity, V_E [47].

$$V = V_{\mathrm{E}} \exp\left(-\frac{\rho_0}{2B\beta \sin(\gamma)} \mathrm{e}^{-\beta y}\right) \tag{4.4}$$

Using similar assumptions, the maximum deceleration can be calculated along with the altitude and velocity where the maximum deceleration occurs. Similarly, if Eq. 4.4 is combined with a model for convective heating, or other properties, the maximum value of the convective heating may be determined along with its corresponding altitude and velocity [47]. (Note that Allen and Eggers suggest that the entry flight path angle, γ_E, be used for the constant flight path angle [47], but the correct value to maximize reliability is often difficult to determine. A modern method for the determination of the optimal flight path angle to be used for the Allen-Eggers approximation is given in [45].)

The Allen-Eggers approximation gives a simple relation between altitude and velocity for a ballistic reentry that is reasonably accurate compared to the true trajectory solution without relying on numerical methods to solve the full motion equations. This

results in a computationally low-cost method to obtain estimates for trajectories. This is useful for during the conceptual design process, but also is useful on flight missions for on-board rapid trajectory calculations. However, there are several factors that hold this approximation from achieving higher levels of accuracy. Mainly, the assumption that flight path angle is constant is not realistic for shallow entry angles lower that 7 degrees [45]. Gravitational effects also become more significant at these lower entry angles. Therefore, it is desirable to use the full equations of motion in the determination of the reentry trajectory.

While no closed-form solution exists for the full planar equations of motion (Eqs. 4.1, 4.2 and 4.3), numerical methods can be employed to obtain a solution. Using MATLAB's `ode45` solver [48], a trajectory estimator was developed that, when provided the entry altitude, y_E, entry velocity, V_E, entry flight path angle, γ_E, and the vehicle ballistic coefficient, B, produced the full vehicle trajectory. This alternate method improves slightly on the Allen-Eggers method, particularly for low entry flight path angles. While this method is more computationally expensive than the Allen-Eggers approximation, the increase (from approximately 0.005 seconds to approximately 0.33 seconds run time) is negligible for the purpose of making intermittent conceptual design choices.

4.1.2 Flow Environment Along the Trajectory

Once the full trajectory is calculated, the software computes the heat-flux, wall temperature, and dynamic pressure at the notional stagnation point of the vehicle assuming zero angle-of-attack at each point along the trajectory. The vehicle geometry is included in the calculation by means of a nose radius, assuming a spherical cap. Heat flux is calculated using the Sutton-Graves heat flux model, shown in Eq. (4.5) [49, 50]. This model gives the radiative heat-flux that expels heat from the surface of the body to free space for a given nose radius, R_{n}, where k is Sutton-Graves constant for Earth (k =

1.7415×10^{-4} kg$^{1/2}$/m), ρ is the atmospheric density, and v is the vehicle velocity.

$$q_{w,s} = k \left(\frac{\rho}{R_{\mathrm{n}}} \right)^{\frac{1}{2}} V^3 \tag{4.5}$$

Wall temperature is calculated assuming radiative equilibrium – the vehicle expels all heat-flux via irradiation – and using the Stefan-Boltzmann equation, shown in Eq. (4.6) [50]. Here, σ is the Stefan-Boltzmann constant, and ϵ is the emissivity of the candidate TPS material, which is around 0.9 for TUFROC [51], a candidate TPS material for HyCUBE.

$$q_{w,s} = \epsilon \sigma T_{w,s}^4 \tag{4.6}$$

Dynamic pressure was calculated from the velocity and density using Eq. (4.7) [52].

$$p = \frac{1}{2} \rho V^2 \tag{4.7}$$

The advantage of such software is the ability to run many cases varying a design parameter and obtain an almost instantaneous result to evaluate design decisions without waiting for a fully-resolved CFD solution. This estimator software was used to inform design decisions of the thermal protection material and evaluate the effect of various design parameters on mission performance.

4.1.3 Validation of Estimator vs. Industry Standards

The stagnation point estimator was validated against outputs from TRAJ [53], a NASA high-fidelity simulation tool, in order to determine its accuracy. TRAJ is a three degree of freedom (3DoF) trajectory simulator that integrates the equations of motion using the Runge-Kutta method. It also includes sophisticated aerothermodynamic models or atmospheric property databases to predict the aerothermal environment along a trajectory [54, 55].

A comparison was performed for a HyCUBE-like case, with a ballistic coefficient of 254 kg/m^2, a nose radius of 5 cm, an entry velocity of 7.5 km/s, an entry altitude of 100 km, and several small flight path angles. The comparison between the two

methods, shown in Fig. 4.1, shows two TRAJ outputs using different heat flux models (Brandis [56], and Fay-Riddell [57]) and the output of the estimator for the same vehicle parameters with three different entry flight path angles, γ. Each color represents a different entry flight path angle case (2°, 5° and 10°).

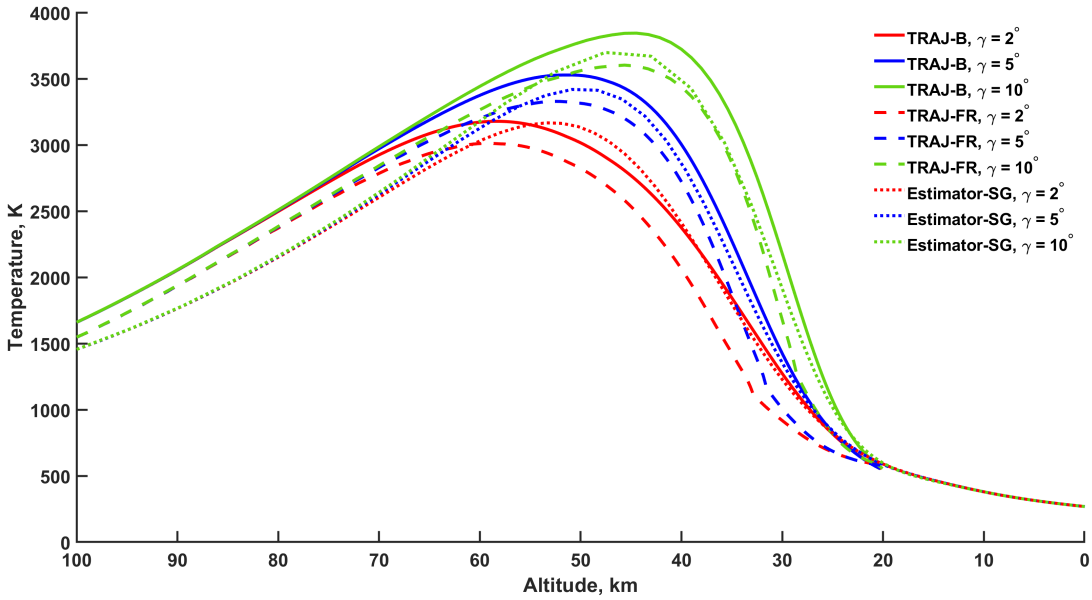

Figure 4.1: Stagnation temperature for $B = 254$ kg/m^2, $R_n = 5$ cm, $v_E = 7.5$ km/s. Comparison of closed form estimator with the outputs of TRAJ for several entry flight path angles.

The results of this comparison indicate that the simple tool gives a reasonably accurate answer for all three cases. The smallest γ case does show some difference between the estimator and the TRAJ outputs, as the peak temperature occurs lower in the atmosphere than the TRAJ peak temperatures. This is caused by a difference in atmospheric density models used to calculate the two trajectories, as it was also observed that the estimator's trajectory enters slightly deeper into the atmosphere than the TRAJ trajectory before losing velocity for this case. However, the peak temperatures are comparable to the TRAJ outputs. These results lend confidence to the stagnation point estimator's validity in guiding design considerations. With regard to entry angle, the key takeaway

is that stagnation temperature increases significantly as entry angle increases. Therefore, to minimize heating on the vehicle, a shallow entry angle is desirable.

4.2 High Fidelity Computational Fluid Dynamics

High fidelity computational models were used to create an aerodynamic database for the 3U format design. To fully span the potential flow conditions seen in Fig. 1.1, as well as to gather information about the initial flight from the ISS to the regime of interest, simulations were run at set conditions spanning 40 km to 300 km in altitude, 4 to 8 km/s in velocity, and 0° to 90° in angle of attack.

Simulations at *high altitudes* in the rarefied regime were performed with the MGDS solver that uses the Direct Simulation Monte-Carlo method [58–60]. The collisional physics in the DSMC method for the high altitude regime simulations used a 5-species model. This model was used for all conditions because the flow at high altitudes is essentially collisionless. Thus, the particle-surface collisions are dominant in determining the forces on the body while the gas-phase collision rate is very low. Using an 11-species model for high altitude simulations simply increases the computational expense in order to produce fully sampled solutions while no appreciable change in surface forces and moments is observed. However, the computational grid was over-refined to a much smaller size than the freestream mean free path such that it could resolve the surface physics.

At lower altitudes where the flow is expected to be in the continuum regime, computational fluid dynamics (CFD) was used to obtain the forces and moments acting on the vehicle in select cases and to obtain flow conditions surrounding the 3U body shape. The US3D hypersonic flow solver was used to perform these simulations, and the 11- and 5-species models were employed selectively based on the flow conditions [61, 62]. Multiple grids were constructed to properly resolve the flow and surface physics. In the so-called *transitional regime* both methods were used to obtain aerodynamic force and moment results. The vehicle surface was modeled as an isothermal wall at 800 K for all simulations, as an initial estimate while gathering information about the flowfield and

body forces. Later decisions about the TPS and surface properties will allow a model of the surface temperature to be used in the high-fidelity CFD simulations, to further improve the predictions of peak-heating and gas reactions near the body.

4.3 Results and Implications

4.3.1 CFD Results

The final aerodynamic database was built by recognizing that the data admit a normalization involving the dynamic pressure (Eq. 4.7), and using, by convention, the frontal area and the length of the vehicle. The normalization allows for universally calculating the forces and moment (as shown in Fig. 4.2) – when used for dynamic response simulations – by simply making the coefficients functions of the flow conditions, density and velocity magnitude, using Eq. 4.8. The coefficients are fitted as functions of ρ and V from the normalized simulation results. The coefficient of drag along the body axis, for example, is calculated as:

$$C_x = \frac{F_x}{\frac{1}{2}\rho V^2 A} \tag{4.8}$$

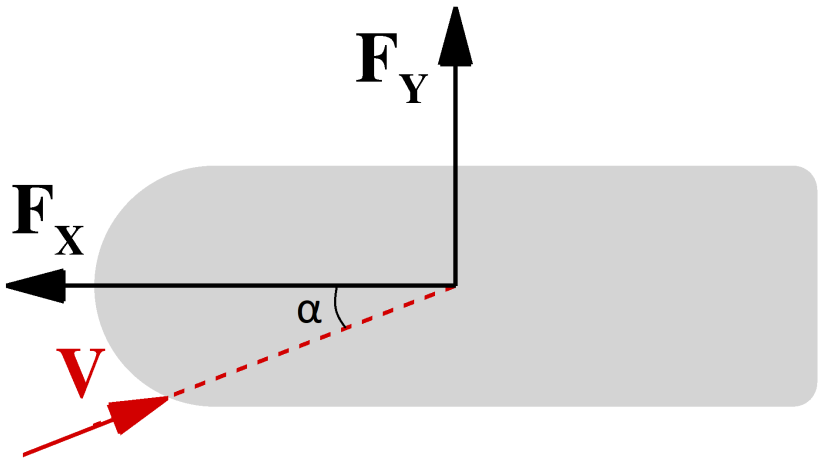

Figure 4.2: The direction of axial and normal forces relative to the angle of attack, α.

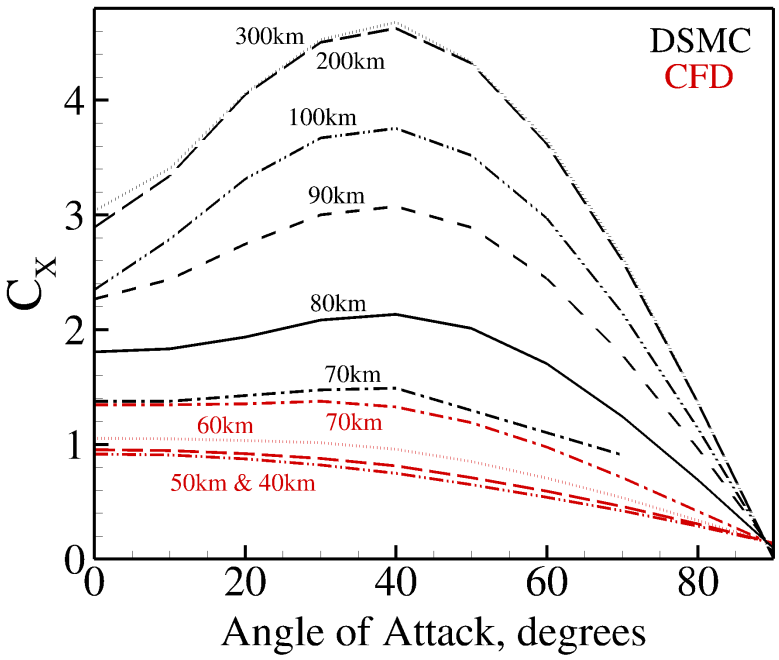

Figure 4.3: Coefficient of axial drag as a function of angle of attack and altitude.

This database of solutions (seen in Fig. 4.3) is dependent upon the three variable "inputs" of altitude, angle of attack, and velocity, and provides estimates of the aerodynamic coefficients that can be used to calculate the ballistic coefficient (Eq. (3.1)). The black lines represent results from DSMC and the red lines represent results from CFD. Due to the normalization of C_x by velocity, the coefficients, C_x, C_y, and C_{Mz}, collapse to a single curve for each altitude. The axial drag coefficient generally decreases as the vehicle descends deeper into the atmosphere, but can either increase or decrease with angle of attack depending on its current atmospheric regime. In the continuum regime, the coefficient decreases with angle of attack. However, in the transitional and rarefied regimes, the coefficient increases with angle of attack until about 40 deg, then decreases with further increasing angles. The coefficient was found to range between 0.8 and 3.5 in the range of altitudes of the reentry portion of the trajectory and for "moderate" angles of attack (less than 40 degrees). An interpolation between the aerodynamic coefficients

can be computed from these results, which will provide a function for the changing ballistic coefficient. This will improve the estimates made by the closed-form solutions discussed in the following section as well as inform considerations of vehicle dynamics and stability.

The results from the high-fidelity computational models were also used to understand the three-dimensional aerothermal environment surrounding the HyCUBE vehicle. Solutions were produced at a variety of points along the projected vehicle trajectory for a range of angles of attack. Figs. 4.4, 4.5, and 4.6 show the distributions of temperature, pressure, and mass fractions of dissociated gas species around the vehicle for a representative case.

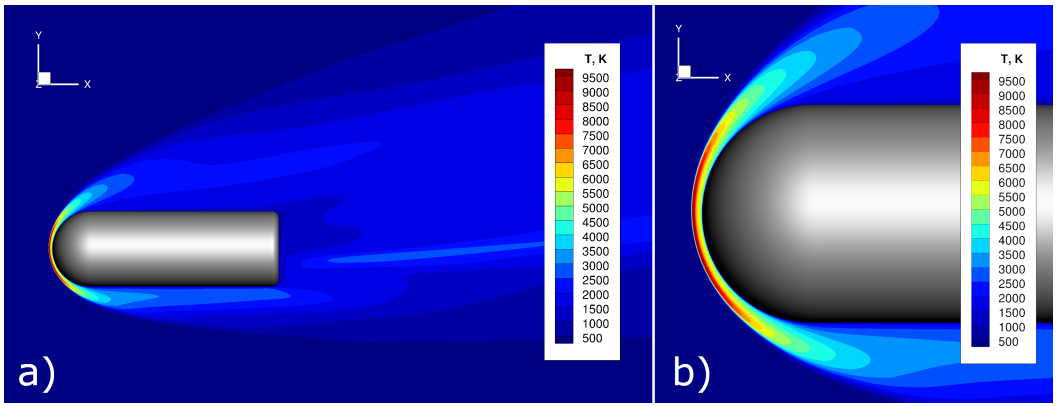

Figure 4.4: The a) full temperature field surrounding the HyCUBE vehicle and b) enlarged temperature field surrounding the HyCUBE nose. Results shown are for flight conditions of 50 km altitude, 4.7 km/s velocity, and 10 degrees angle of attack.

Fig. 4.4 shows that the area of highest temperature, reaching almost 10,000 K, is located immediately behind the bow shock and centered around the stagnation point. The high temperatures downstream of the shock will lead to the formation of N, O, and NO as well as thermal nonequilibrium. The gas species content in this region will be characterized experimentally by the spectrometer. The temperature decreases rapidly along the stagnation streamline as the wall is approached and also as the flow moves around the nose. While the simulations assume a uniform surface temperature of 800 K, which is not indicative of the experimental surface temperatures, the wall-normal

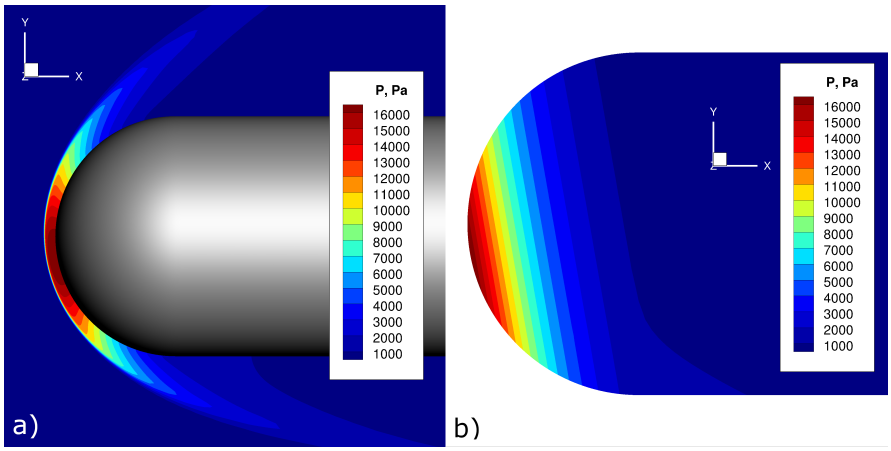

Figure 4.5: The a) flow pressure field and b) surface pressure distribution of the HyCUBE vehicle under flight conditions of 50 km altitude, 4.7 km/s velocity, and 10 degrees angle of attack.

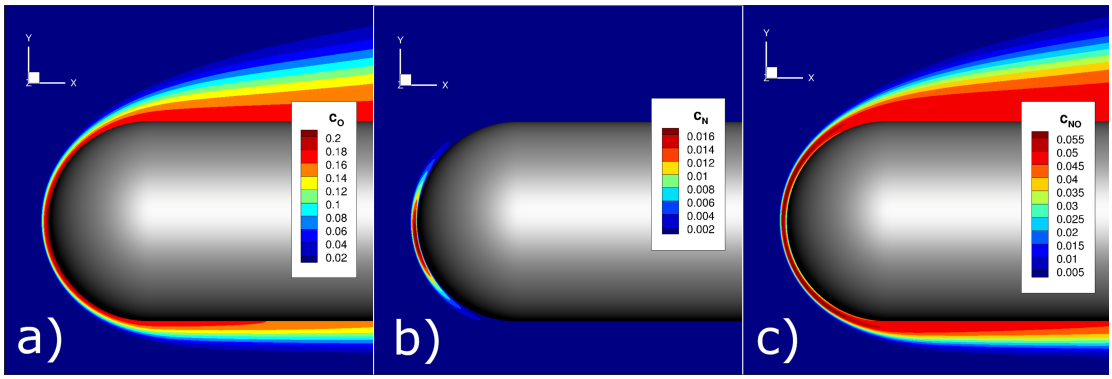

Figure 4.6: Mass fraction of a) O b) N and c) NO for the flight conditions of 50 km altitude, 4.7 km/s velocity, and 10 degrees angle of attack.

heat flux can be compared against experimental values derived from thermocouples. Similarly, the area of highest static pressure, reaching 16 kPa, is located behind the shock and centered around the stagnation point, as shown in Fig. 4.5a. This high pressure region extends to the wall, as is shown by the surface pressure distribution in Fig. 4.5b. HyCUBE's pressure transducers will characterize this distribution at discrete locations.

The CFD analysis showed that the dissociated gas species of interest, N, O, and

NO, will present in the flowfield around the HyCUBE vehicle. Fig. 4.6 shows the mass fraction of each of these dissociated species. Note the different color scales for each molecular species – elemental oxygen, for example, is more than ten times as abundant in mass than elemental nitrogen at the stagnation point. In Figs. 4.6a and 4.6c, it can be seen that O and NO are present in large quantities around the entire vehicle body. However, Fig. 4.6b shows that N will only be present in significant quantities at the stagnation point, making this location the area of most interest for a spectrometer measurement. Another observation is that the dissociated species, specifically O and NO, persist in significant quantities very far downstream even as the flow pressure and temperature have nearly returned to their freestream values. This underscores the nonequilibrium character of the flowfield and identifies another region of the flow that may be worthy of further data collection, beyond the stagnation point region. Table 4.2 gives the number density of the five species included in the CFD analysis for these two regions: the stagnation point region and a region 90° downstream from the stagnation point. This table shows that species like NO and O are present in significant amounts in the downstream region; the number densities in the downstream region are on the same order of magnitude as those in the stagnation region.

Gas Species	Number Density at Stagnation Point	Number Density Downstream
N_2	1.31×10^{20} m^{-3}	2.37×10^{19} m^{-3}
O_2	2.95×10^{18} m^{-3}	1.05×10^{18} m^{-3}
NO	9.30×10^{18} m^{-3}	1.37×10^{18} m^{-3}
N	6.26×10^{18} m^{-3}	8.03×10^{14} m^{-3}
O	5.91×10^{19} m^{-3}	9.57×10^{18} m^{-3}

Table 4.2: Number density of gas species at different regions behind the bow shock for flight conditions of 50 km altitude, 4.7 km/s velocity, and 10 degrees angle of attack.

The CFD results were used to determine the required measurement range of sensors as well as the optimal arrangement of sensors during the sensor selection process. This process will be discussed in detail in Chapter 5.

4.3.2 Stagnation Point Estimator Results

The inputs for the stagnation point estimator are ballistic coefficient, nose radius, and the initial conditions vector: entry altitude, entry velocity, and entry flight path angle. The ballistic coefficient and nose radius for the 3U concept are $B = 200$ kg/m^2 and $R_\mathrm{n} = 5$ cm, as mentioned previously. The initial conditions of the trajectory are largely dictated by the launch method. The launch method for HyCUBE was assumed to be an International Space Station (ISS) deployment, which is a common launch method for CubeSats. The orbital velocity of the ISS is 8 km/s, and the vehicle will maintain much of that velocity throughout its orbital stage and into its reentry, thus entry velocity is assumed to be $V_\mathrm{E} = 8$ km/s. Preliminary orbital analysis that is outside the scope of this paper, predicted that the entry flight path angle for such a launch would be around $\gamma_\mathrm{E} = 1°$. The entry altitude is defined as $y_\mathrm{E} = 120$ km, at which point the vehicle becomes non-negligibly affected by the atmosphere. The altitude-velocity mappings for these input conditions are plotted in Fig. 1.1 for the two HyCUBE formats considered. Note that the 3U format enters the continuum regime (80 km) at high speed compared with the defined region of interest and decelerates to 4.7 km/s at 50 km, which is the condition depicted by the temperature, pressure, and concentration fields in Figs. 4.4–4.6. By contrast, the stronger drag forces and smaller ballistic coefficient associated with the 12U format lead to lower speeds through the region of interest. The approximate times over which the 3U and 12U formats descend from 80 km to 50 km are 156 s and 104 s, respectively.

Preliminary CFD results indicated early on in the design process that HyCUBE would experience heat fluxes that would challenge the capabilities of even the most robust non-ablative materials. A material known as TUFROC (Toughened Unipiece Fibrous Reinforced Oxidation-resistant Composite) was identified as being a prime candidate due to its high heating limits while remaining non-ablative. TUFROC is rated for wall temperatures up to 2000 K and dynamic pressures up to 5 kPa, making it one of the most robust non-ablatives available [51]. The estimator results, however, revealed that the original 3U concept was exceeding even this robust material's temperature and

pressure limits, as seen in Figs. 4.7 and 4.8. The stagnation point wall temperature exceeds the TUFROC limit of 2000 K at an altitude of 85 km, peaking just below 2900 K at around 57 km altitude. Similarly, the surface dynamic pressure exceeds the 5 kPa limit starting around 60 km and reaches its peak of almost 17 kPa at around 43 km altitude.

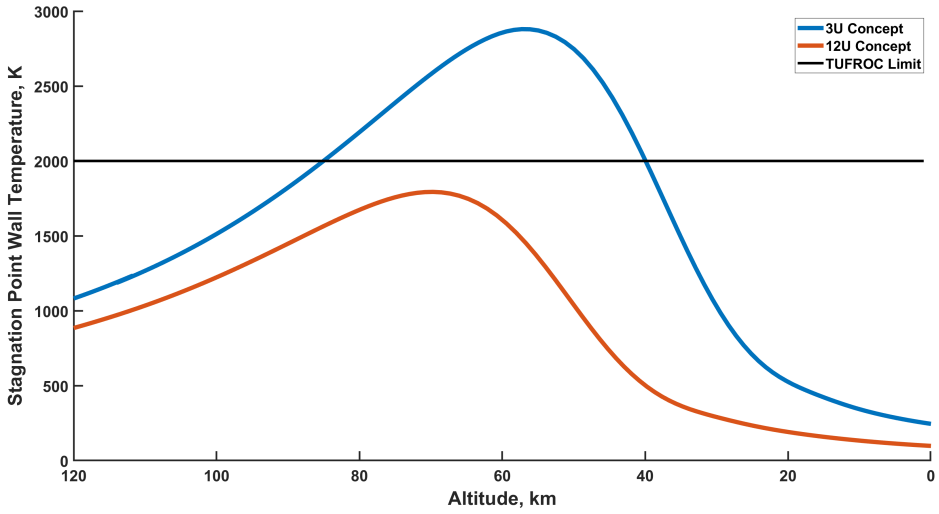

Figure 4.7: Stagnation point temperature along the trajectory of HyCUBE, compared to the rated limit of TUFROC.

Efforts were made to reduce the stagnation temperature and pressure by adjusting various simulation inputs. First, the entry flight path angle and entry velocity were evaluated. Further orbital simulations predicted the entry flight path angle could be reduced to 0.2°, a reduction from 1°, which had been previously assumed in early simulations. Entry velocity was varied in simulations to determine the reduction that would be required to reduce the stagnation temperature and pressure to acceptable limits, and the feasibility of such a variation was discussed. As these parameters are largely determined by the launch conditions, they are relatively inflexible in practice. Both of these parameters, however, were relatively ineffective in reducing the peak conditions. For instance, the change in entry flight path angle from 1° to 0.2° reduced the maximum stagnation point wall temperature by only several degrees Kelvin. Even a drastic

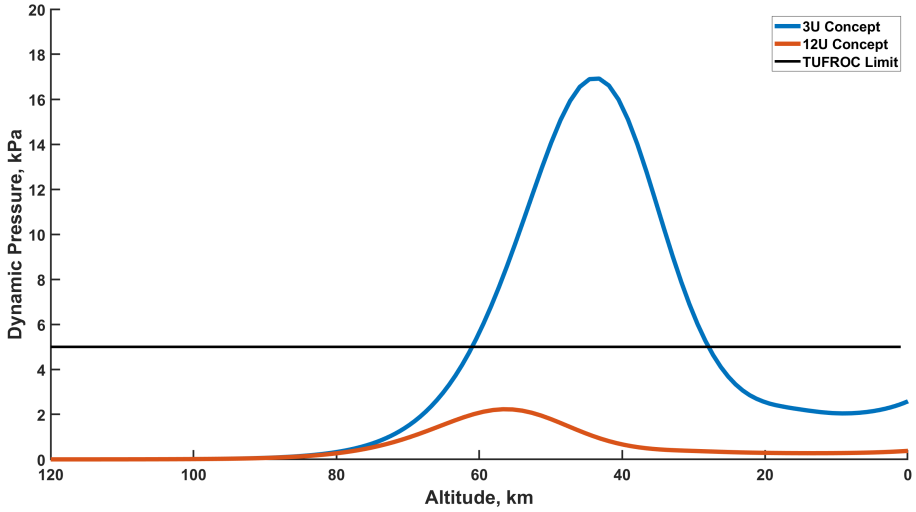

Figure 4.8: Stagnation point pressure along the trajectory of HyCUBE, compared to the rated limit of TUFROC.

(and, in terms of meeting the flight regime requirements of the mission, unfeasible) decrease in entry velocity from 8 km/s to 5 km/s only brought about a reduction of the stagnation point wall temperature to just under 2600 K, still vastly exceeding the TPS temperature limit. Varying these parameters was similarly unsuccessful in reducing the stagnation pressure below the TPS pressure limit. Further, it was discovered that based on the Sutton-Graves heating model, the current vehicle form factor would not be able to achieve the goal conditions (Fig. 1.1) while remaining compliant with the TUFROC limits. This was due to the small nose radius of the vehicle and the relatively high velocity within the region of interest. The maximum stagnation point wall temperature would always exceed 2000 K as the vehicle passed through the region of interest, regardless of the entry velocity or flight path angle. Thus, other parameter changes were required to make the vehicle compatible with TUFROC.

The next parameters to be explored were the ballistic coefficient and nose radius of the vehicle. These parameters affected the conditions much more strongly than entry velocity and entry flight path angle. Still, changes to both parameters were needed to bring the conditions under TUFROC limits. For instance, reducing the ballistic

coefficient from 200 kg/m^2 to 30 kg/m^2, brought the maximum pressure under the 5 kPa TUFROC limit, but the maximum temperature decreased only to around 2200 K. By also increasing the nose radius from 5 cm to 25 cm, however, it was shown that the maximum stagnation point temperature could be reduced to less than 1800 K and the maximum stagnation point pressure could be reduced to less than 3 kPa. Similarly, only increasing the nose radius was not enough to become TUFROC-compliant; both parameters needed to be adjusted in order to meet the pressure and temperature limits. Through this combination of input adjustments, it was shown that the limits could be met, which showed a non-ablative environment was still possible.

To achieve these new requirements for nose radius and ballistic coefficient, multiple design modifications were considered. Reducing the mass of the 3U design was the first option considered. This, however, was not feasible, as the 4 kg mass requirement was already a challenge to meet with the desired hardware for HyCUBE. Thus, an increase in vehicle cross-sectional area was considered, forcing a deviation from a 3U concept. A drag skirt was added to increase cross-sectional area as well as to add drag, making possible such a drastic drop in ballistic coefficient to 30 kg/m^2. An increase in body cross section to a 2U$\times$2U scale, combined with the drag skirt, allowed for an increased nose radius to 25 cm without creating any sharp discontinuities at the vehicle shoulder. These design changes result in decreases in stagnation point pressure and temperature for the redesigned concept which are also shown in Figs. 4.7 and 4.8. As can be seen there, these results indicate that the new concept will comply with the limitations of the TUFROC TPS material and achieve the targeted regime of interest in Fig. 1.1.

Chapter 5

Sensor Pod Design

5.1 Design Requirements and Considerations

During the design of the HyCUBE sensor pod, several requirements dictated design choices. First, it was imperative to comply with CubeSat requirements for size and weight. As previously mentioned, there are standard CubeSat configurations, such as 1U, 3U, 6U, and 12U, that have the most readily available flight opportunities. Thus, in order to meet the mission goal of being cost-effective and able to achieve multiple flights, adhering to one of the standard form factors was strictly necessary. Each CubeSat form factor also has guidelines for the allowable mass of the vehicle, which also needed to be considered in our design process. For instance, a 3U CubeSat must have a maximum mass of 6 kg [63]. However, this mass requirement is less stringent than the size requirement, as there can be exceptions made on a mission-by-mission basis. There are also restrictions for the location of the center of mass of the vehicle. Again for a 3U vehicle, the center of mass must be within 2 cm of the geometric center of vehicle's x and y axes (length and width axes) and within 7 cm of the geometric center of its z axis (height axis) [63].

Besides the requirements on the vehicle size and mass, there were desired design elements to be considered. In order to simplify the flow chemistry, it was desired that the vehicle utilize an inert, non-ablative thermal protection system. The use of an

reactive or ablative material, while acceptable if needed to ensure vehicle survival, would introduce additional gas species and ablation products into the flow that would make the determination of the reaction rates of the chemical processes of interest (dissociation and recombination of nitrogen and oxygen species) more difficult. Thus, a key design aspect was determining the feasibility of using a non-ablative TPS material.

5.2 Thermal Protection System

As mentioned in the previous section, the use of a non-ablative TPS material is highly desirable to simplify and improve the data reconstruction of chemical reaction rates. As discussed in section 4.3.2, a material known as TUFROC (Toughened Unipiece Fibrous Reinforced Oxidation-resistant Composite) was identified as a candidate TPS as it was a non-ablative material with the ability to withstand conditions as well as or better than any other non-ablative material. TUFROC utilizes two layers of TPS material, an outer ROCCI (Refractory Oxidation-resistant Ceramic Carbon Insulation) cap layer, made of a silicon oxycarbon matrix and carbon fiber, and an inner insulating silica layer, typically Alumina Enhanced Thermal Barrier (AETB) [64]. During arcjet testing, TUFROC was demonstrated to be an effective TPS option for surface temperatures up to 2000 K and up to 5 kPa [51, 65]. The thickness of TUFROC to be used for HyCUBE remains an unknown. The blunt variations of TUFROC artifacts used in testing were 2 inches thick [51], but further analysis must be done to determine the required thickness for the specific mission, including the thickness of each of TUFROC's layers. The FIAT software from NASA Ames is being explored as a candidate for sizing the TPS material [66].

Another open question regarding TUFROC is its ability to be instrumented and maintain its structural and thermal integrity. All tests thus far have been performed with completely intact test bodies, and it remains to be seen what effect disturbances in the TPS (like pressure taps or spectrometer viewing windows) might have on the flow conditions and material integrity. In testing, thermocouples were placed at the interface between the two TUFROC layers, but further investigation is required to determine if

installation at other in-depth locations will affect material performance [51].

5.3 Desired Sensor Suite

As understanding of chemical kinetics is a key science goal for the HyCUBE mission, it is desired that the HyCUBE sensor suite collect the emission spectra of the flow that will give the relative gas species fractions. Additionally, the sensor suite will take direct readings of aerothermodynamic properties, specifically surface temperature and dynamic pressure. These readings will be used also to calculate the heat flux and surrounding density. Together, these parameters will be able to give valuable data for the gas species densities as well as their temperature states which will be used to validate models for chemical reaction rates and molecular relaxation rates.

5.4 Sensor Selection

Currently, only the 3U vehicle design has been fully analyzed using CFD methods to find the off-stagnation environmental conditions that will need to be measured. Thus, the sensors proposed here will be for that design. The 12U vehicle designed will be fully analyzed in the future using the same design processes that have been described in Chapter 4.

Sensor	Vendor and Model	Size & Mass	Measurement Range
Spectrometer	Ocean Insight STS-UV	$40 \times 42 \times 24$ mm 68 g	190-650 nm
Pressure	Kulite XCQ-080 or XCE-080	$\varnothing$ 2 $\times$ 6 mm 0.4 g	0-35 kPa
Thermocouple	Type K or S	n/a	0-1550 K or 0-1750 K

Table 5.1: Proposed sensors and general specifications.

To characterize the gas species content near the HyCUBE surface during its descent, a spectrometer will probe a line of sight normal to the vehicle surface near the stagnation point. The spectrometer will aim to observe the presence and relative number density of N, O, and NO in this zone (as seen in Fig. 4.6) by focusing on the UV wavelength range

[14]. The exact viewing location will be determined using spectral predictions based on results of US3D solutions coupled with NASA's NEQAIR software. This software takes the gas content around the vehicle and integrates the spectral emission along a line of sight to build a predicted measurement from the spectrometer. The candidate spectrometer is the Ocean Insight STS series spectrometer, specifically the STS-UV model, which probes the ultraviolet wavelength range from 190-650 nm. There are other STS models that probe the visible and infrared wavelength ranges. This spectrometer has an optical resolution as low as 1 nm, depending on the chosen width of the entrance slit. This series of spectrometer has been used in previous CubeSat missions, as it was used on the QARMAN and SASSI^2 missions. The specifications for this instrument can be found in Table 5.1.

Pressure on board HyCUBE will be measured using pressure transducers with taps distributed across the nose cap of the vehicle. High-fidelity simulations from US3D were used to create a three-dimensional solution of the surface dynamic pressure at several representative cases along the HyCUBE trajectory. These simulations showed that the stagnation point pressure reached a maximum of 20 kPa along the proposed 3U-format trajectory (see Fig. 1.1). This led to the choice of a pressure sensor with a maximum limit of 35 kPa. The off-stagnation point conditions were significantly lower than the stagnation conditions, indicating that a more sensitive sensor could be used away from the stagnation point. However, because it is not known at what angle of attack or angle of roll HyCUBE will fly, the same sensor range of 35 kPa was chosen for all pressure sensors. A pressure transducer that has been identified as one candidate is the Kulite XCQ (general performance) or XCE (optimized for high-temperature) series of miniature pressure transducers. These sensors are small enough to include multiple sensors even with HyCUBE's small form-factor and meet the criteria for measuring pressures from 0-35 kPa. See Table 5.1 for general specifications.

Temperature will be measured at discrete locations by thermocouples. Similar to the pressure sensors on board HyCUBE, thermocouples will be distributed across the vehicle nose in order to maximize the flowfield information that can be gathered. Given the high surface temperatures for both 3U and 12U formats and the need for robust

instrumentation, the thermocouples will likely be embedded in the TPS material, at a known depth. Thus, surface temperatures would need to be estimated indirectly from the measurements. This ensures the maximum temperature of the sensor will not be exceeded, as well as ensure the structural integrity of the sensor mount. Type S, which is rated for 1750 K, and type K, rated for 1550 K, thermocouples are being considered [67]. Thermocouple "stacks," in which multiple thermocouples are embedded at different depths along the same radial line of sight, are also being considered. These stacks would allow for a local heat flux measurement to be determined. No specific vendor or model of thermocouple has been identified as a candidate sensor for HyCUBE.

5.5 Sensor Orientation and Arrangement

5.5.1 Spectrometer Orientation

One option for the spectrometer orientation is to place it such that its viewing region is directly in front of the geometric center of the nose, which is the nominal stagnation point of the flow. This is so the collection of dissociated species is maximized. As can be seen in Fig. 4.6, some species (N) do not persist in significant amounts downstream of the stagnation point. Therefore, in order to maximize the collection of all species of interest, the spectrometer will face out of the nose towards the stagnation point. A preliminary result from NASA's NEQAIR software looking out of the nose is shown in Fig. 5.1. This predicted spectrum indicates that there will be observable transitions occurring in the UV range which the spectrometer will probe.

An alternative placement of the spectrometer that could yield interesting and useful results is to orient the viewing path at a location 40°–90° downstream from the stagnation point. This region is of interest due to the strong nonequilibrium behavior of the flow. As seen in Figs. 4.4 and 4.6, the employed computational chemistry model predicts some dissociated species (O and NO) persist significantly downstream of the stagnation point, even while high temperatures do not persist in the same region. Thus, it would be interesting to probe the chemical reactions and recombinations in this region to examine this nonequilibrium behavior.

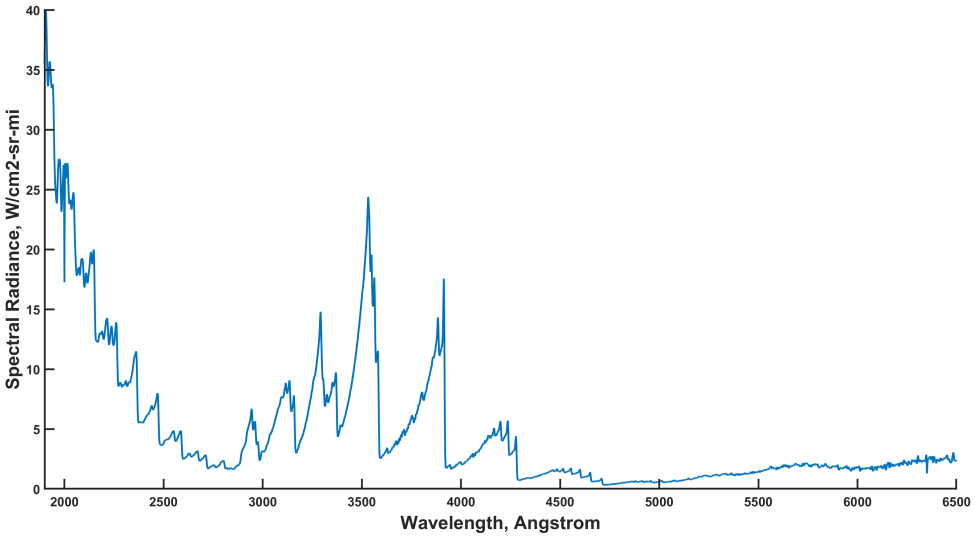

Figure 5.1: NEQAIR prediction of the emission spectrum that will be collected by the STS-UV spectrometer looking out of the vehicle nose, as produced by the NEQAIR software. This spectrum was produced for a case at 60 km altitude, 6.3 km/s velocity, and 0 degrees angle of attack. Note that the NEQAIR software uses a wavelength resolution of 0.1 Angstrom, which is several orders of magnitude smaller than that of the spectrometer.

5.5.2 Pressure Sensor Arrangement

The number and arrangement of pressure sensors were also evaluated. Pressure measurements at multiple streamwise and circumferential locations are desired to characterize the overall pressure field for comparison against simulations. A second consideration was determining a sensor arrangement that could be used to determine angle of attack over a wide range of actual angles of attack and roll orientations. To simulate collected in-flight data, pressure values were extracted at proposed sensor locations and a surface was fitted to these data points. To do this, the Cartesian pressure field on the vehicle surface was mapped onto a polar coordinate space $p(\theta, \phi)$. The body angle, θ, is the angle from the HyCUBE nose, where 0 degrees is the tip of the vehicle's nose and 90 degrees corresponds to the vehicle's shoulder. The circumferential angle, ϕ, is the angle from an arbitrarily chosen quadrant of the vehicle (since the vehicle has rotational

symmetry). This polar coordinate space is then recast into a two-dimensional Cartesian system, $p(\eta, \zeta)$, in order to do the fitting in a simpler coordinate space, but all discussion will be presented in terms of the polar coordinate system.

$$p(\theta, \phi) = a \cdot \exp\left\{ - \left[\left(\frac{\theta - b}{c} \right)^2 + \left(\frac{\phi - d}{e} \right)^2 \right] \right\} + f \tag{5.1}$$

It was observed that a Gaussian surface (Eq. 5.1) could be fitted to the simulated sensor data to recover the stagnation point and the pressure field near it, as seen in Fig. 5.2. Since the location of the stagnation pressure corresponded to the angle of attack of the vehicle, the accuracy of the fitting method could be evaluated with regard to predicted angle of attack. To evaluate a potential sensor arrangement, the angle of attack predicted by the Gaussian fit were compared to the true angle of attack. Arrangements with six – the minimum number of points for which a Gaussian fit is possible – to nine sensors in many different placement patterns were considered and analyzed for angles of attack from 0 to 40 degrees and all possible roll angles. The best performing arrangements proved to be those with multiple sensors at a larger body angle than all expected angles of attack and those that had sensors distributed across all circumferential angles. These attributes were helpful because these arrangements had sensors relatively near the stagnation point for any possible case to capture the peak pressure and had sensors away from the stagnation point to capture the inflection points of the pressure surface.

"Staggered" distributions, like the one shown in Fig. 5.3, performed well for every angle of attack and roll angle case that was considered and became the frontrunner for the final sensor arrangement. These arrangements feature a sensor at the vehicle nose and rings of sensors at two subsequent body angles. The inner and outer rings' circumferential positions are staggered from one another. These arrangements perform well because the sensors are well-distributed around the nose in both the θ and ϕ directions. It was observed that the best of these staggered arrangements were those with the outer sensor ring at $\theta = 80$ degrees, the largest angle considered, especially for larger angles of attack when compared to arrangements at smaller θ values. However, if

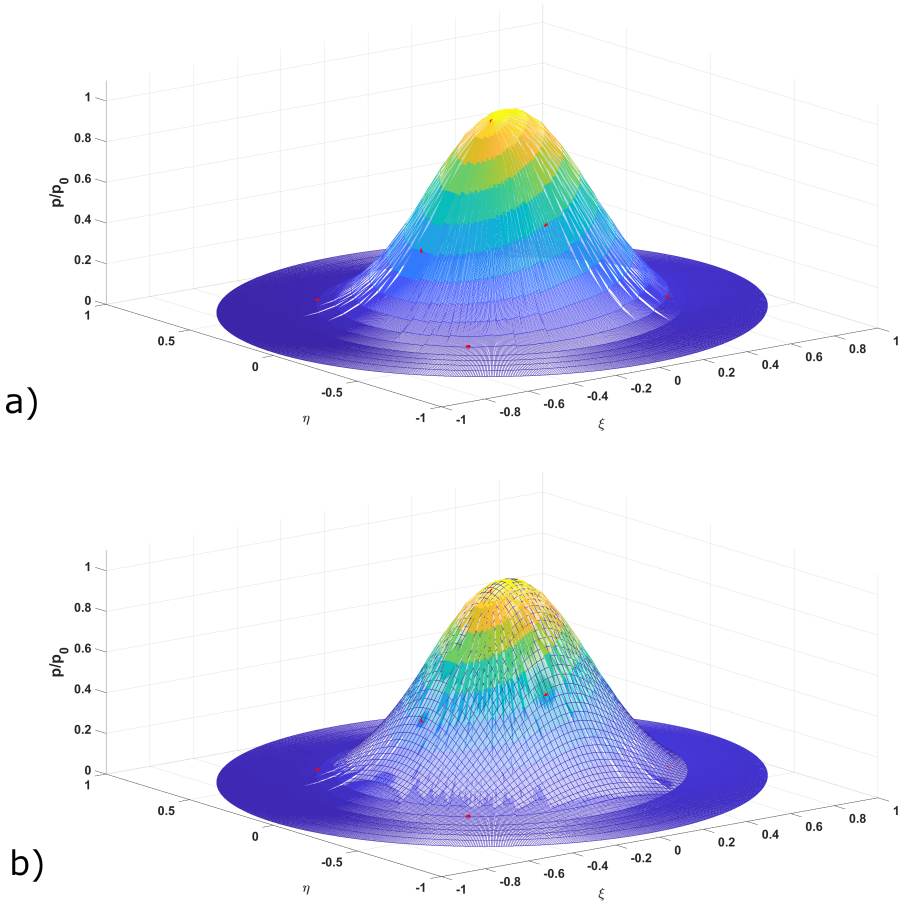

Figure 5.2: The a) pressure distribution across the HyCUBE nose as given by CFD results and b) the pressure distribution overlaid with the Gaussian fit (the lighter grid) to nine sensor locations around the nose. The distribution presented here is for a case at 50 km altitude, 4.7 km/s velocity, and 10 degrees angle of attack. The stagnation pressure, p_0, is approximately 17 kPa.

the inner ring of sensors were also to be moved back to $\theta = 80$ degrees, the arrangement had difficulty predicting small angles of attack. This analysis led to the conclusion that the best performing arrangements were the staggered patterns with the outer sensor ring at $\theta = 80$ degrees and the inner ring of sensors from $\theta = 30 - 70$ degrees.

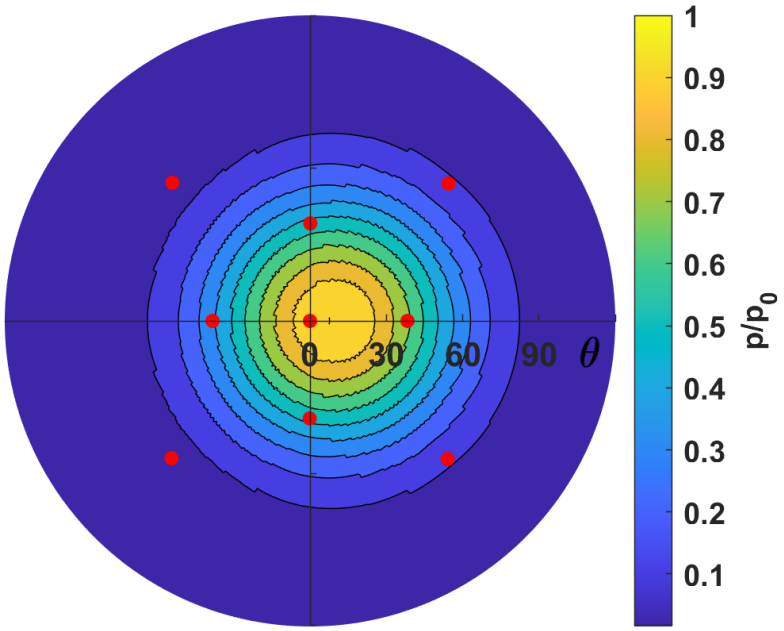

Figure 5.3: Pressure distribution across the HyCUBE nose overlaid with a proposed pressure sensor arrangement. The distribution presented here is for a case at 50 km altitude, 4.7 km/s velocity, and 10 degrees angle of attack. The stagnation pressure, p_0, is approximately 17 kPa.

The results described assumed zero uncertainty in the measurements. An uncertainty analysis was conducted to determine the robustness of the candidate arrangements to random sensor noise. Using a candidate pressure sensor's uncertainty specifications (average of 0.1% of the full scale output, maximum of 0.5%), sensor noise was added into the simulated sensor data before the Gaussian was fitted to it. The fitting was run ten times for each case and the maximum error was recorded. The arrangements with the majority of sensors at large θ values were affected more than those with smaller θ values due to the fact that the sensors at the larger θ values tend to be farther from the stagnation point and have smaller pressure values. Thus, when sensor noise is added, these readings have larger relative uncertainty which affects the accuracy of the fit. Arrangements with the inner ring of sensors closer to the vehicle nose were

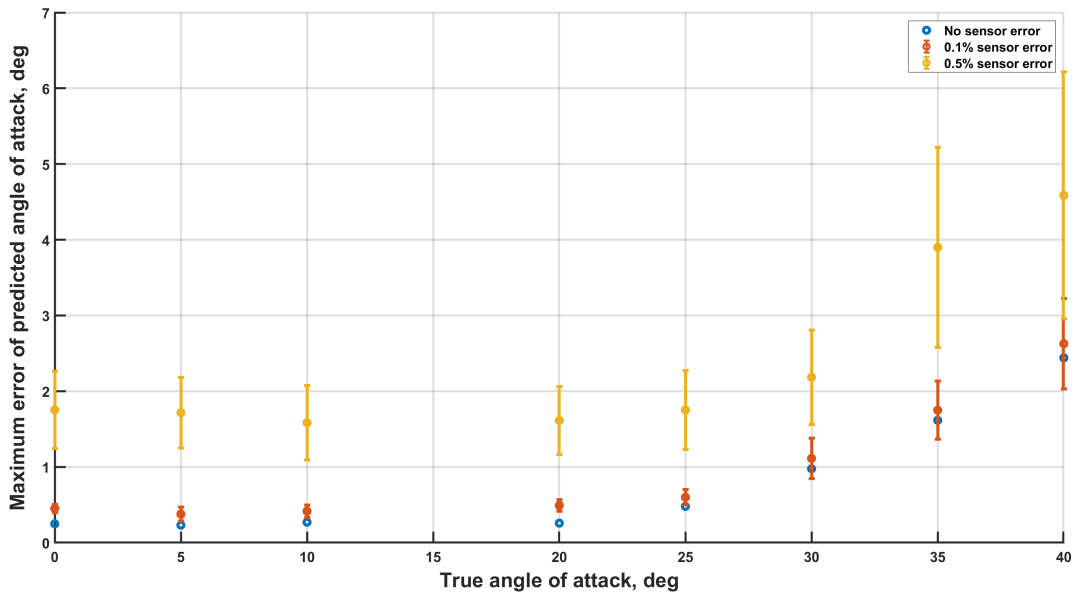

Figure 5.4: Error in estimated angle of attack based on pressure sensor uncertainty for the proposed pressure sensor arrangement.

therefore more robust to sensor noise in estimating angle of attack. Fig. 5.4 shows the uncertainty results for the arrangement with the outer sensor ring at $\theta = 80$ degrees and the inner ring of sensors at $\theta = 40$ degrees, which is the arrangement shown in Fig. 5.3. This arrangement was a top performing arrangement for the nominal fitting and was the best performing arrangement when sensor noise was added. The average maximum error for this arrangement with the typical 0.1% error is less than 3 degrees for any angle of attack case. This corresponds to an error in estimated stagnation pressure of 1.6%.

5.5.3 Thermocouple Arrangement

Similarly to the pressure sensor arrangement, the thermocouple stacks will be distributed across the HyCUBE nose in order to capture the stagnation temperature and the temperatures surrounding it. Less work has been done evaluating fitting of thermocouple data to a three-dimensional surface than has been done for pressure sensor data.

This is due, in part, to the fact that the CFD solutions that have been produced have used an isothermal wall condition and thus do not directly give any useful temperature data. However, heat flux *is* obtained from these simulations, which of course is highly related to temperature. The heat flux data indicates that a similar Gaussian fit may effectively predict the heat flux field, and thus it is likely that the a similar fit could be used for temperature data to determine the optimal thermocouple placements.

As mentioned previously, the thermocouples at the various locations around the nose will by embedded into the TPS material at known depths to create a thermocouple stack. This stack will allow for the measurement of surface and in-depth temperatures but will also allow for a calculation of the local heat flux into the TPS. As the TPS sizing remains to be done, the depths of each thermocouple is unknown at this time.

5.6 Data and Power Budget

The data budget for the proposed sensor suite is shown in Table 5.2. The spectrometer will provide the vast majority of sensor data that must be downloaded from HyCUBE. Each packet of data is 2,111 bytes, of which 2,048 bytes are spectroscopic data. As chemical reaction assessment is a key goal of the mission, the spectrometer will sampled at its maximum frequency of 75 Hz. This rate is limited by the minimum integration time of the spectrometer as it must wait to collect enough emission data to create a spectrum for each sampling. The large data size means that the spectrometer occupies the vast majority of the required data throughput. If needed, the total data requirement must be reduced by decreasing the spectrometer sampling rate. The pressure sensor and thermocouple output a direct voltage and will need to be translated into a digital signal in order to be transmitted. This will be done using a 16-bit digital multiplexer, giving each data packet a size of 2 bytes. This small data size is beneficial because it keeps the data consumption low, even at higher sampling rates. These sensors will be sampled at 300 Hz, and will be calibrated with the spectrometer so that each sensor will take readings at the same time (there will be four pressure and temperature reading for each spectrometer reading).

Sensor	Data Size (Bytes)	Acquisition Rate (Hz)	Data Rate (Bytes/Second)
Pressure Transducer (9x)	2 (18)	300	600 (5,400)
Thermocouple (9x)	2 (18)	300	600 (5,400)
Spectrometer	2,111	75	158,000

Table 5.2: Data budget for the proposed sensor suite.

The power budget for the HyCUBE vehicle is shown in Table 5.3. Similar to the data budget, a large portion of the required power is occupied by the spectrometer, although not to the same degree. Note that the thermocouple is self-powered and thus does not contribute directly to the power consumption. However, the digital multiplexer that is required for the pressure sensors and thermocouples does contribute to the power draw and has been included for completeness. In the case that a second multiplexer would be used to separate pressure and temperature data for simpler connections, this entry will be adjusted as such.

Sensor	Current (mA)	Voltage (V)	Power (W)
Pressure Transducer (9x)	10 (90)	10	0.1 (0.9)
Thermocouple (9x)	- (-)	-	- (-)
Digital Multiplexer	25	3	0.075
Spectrometer	150	5	3.5

Table 5.3: Power budget for the proposed sensor suite.

5.7 Geometric Footprint

As discussed in section 5.1, it is imperative to remain compliant with CubeSat standards for size and weight. The proposed sensors (Table 5.1) have been chosen so that they fit inside the 3U CubeSat form factor. The nine Kulite pressure transducers have a 2 mm diameter and are 6 mm long and weigh 0.4 g. The Ocean Insight spectrometer is 40 mm $\times$ 42 mm $\times$ 24 mm and weighs 68 g. A definitive decision on a model of thermocouple has not been made at this time, but the size and weight of the thermocouples is considered

negligible in comparison with the other sensors.

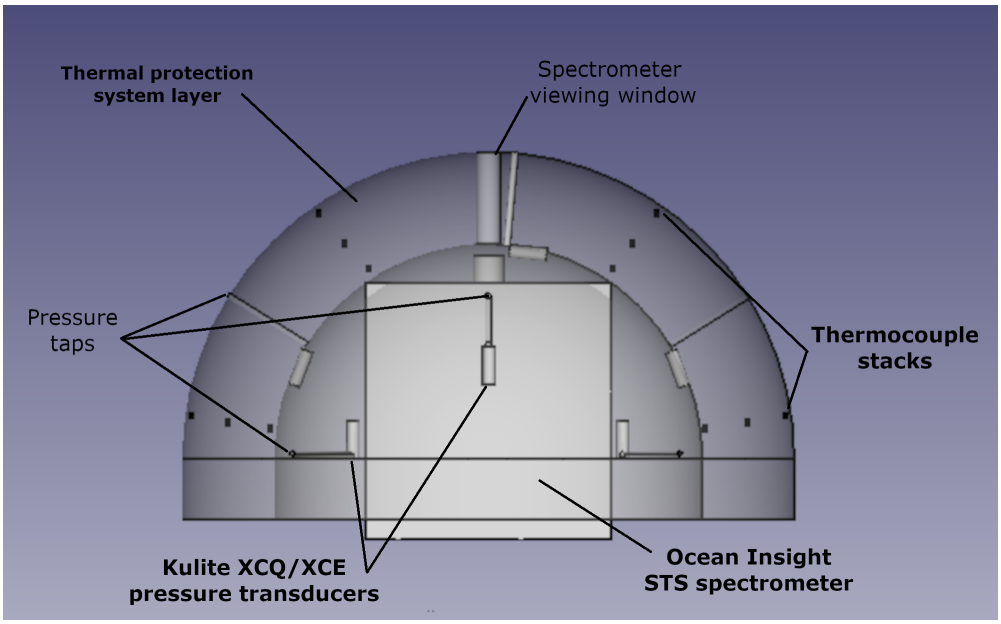

Figure 5.5: Potential sensor configuration within the 3U HyCUBE concept nose. Sensors and thermal protection layer are drawn to scale.

Fig. 5.5 shows a potential geometric footprint of the proposed sensor suite within the nose of a 3U CubeSat. The spectrometer is facing toward the geometric center of the nose, aligned with a viewing window for observation of the flow. The nine pressure transducers are located next to pressure taps arranged in the staggered pattern that was described in section 5.5.2. An alternative layout could be to centralize all the pressure transducers and connect them to the pressure taps via tubing. This may simplify the electronics layout. The nine thermocouple stacks are shown here with three thermocouples making up each stack. These stacks will likely be integrated into thermocouple plugs, made from the same material as the TPS, that will insert into the TPS. As the sizing of the TPS remains an open question, a TPS thickness of 1.5 cm has been utilized (to scale) here.

5.8 Sensor Suite Comparison for the 12U Concept

Much of the analysis and design choices presented thus far have detailed the original 3u HyCUBE form factor. However, if the the redesigned 12U concept is to be considered a candidate in future work, much of the analysis must be repeated for that design. The high-fidelity CFD simulations will be needed to produce the three-dimensional solutions around the new design to inform its measurement environment that may alter the proposed sensor suite as well. For instance, the stagnation temperature and pressure (and thus, the off-stagnation temperatures pressures) will be reduced, which may allow more sensitive sensors to be used to increase measurement accuracy. Also, the gas emission can be expected to change as well due to the decrease in flow temperature. This will reduce the presence of some of the dissociation products of interest, and the orientation of the spectrometer may need to be adjusted.

Another consideration that will require investigation is that of the redesigned concept's aerodynamic stability. If it can be shown that the vehicle stability has improved with the addition of the drag skirt, some off-stagnation sensor may have reduced expected conditions and again a more sensitive sensor may be able to be used.

Finally, the increased size of the redesigned concept may lend itself to the inclusion of more sensors. A secondary spectrometer could be added to observe another flow region, or a different model, like the Ocean Insight STS-VIS visible range spectrometer, could be used to extend the wavelength range being observed. Of course, the amount of pressure sensors and thermocouples around the nose could be increased to allow for more data collection and to add redundancy in case of isolated sensor failures.

Chapter 6

Summary and Conclusions

6.1 Summary of Prior Work and Key Results

The HyCUBE reentry vehicle platform is a novel, low-cost, and efficient means to collect flight data that can provide statistically significant data sets to assess and validate current ground testing methods and computational predictive models. In this thesis, a concept for the HyCUBE Mark-1 sensor pod has been proposed. The sensor pod for HyCUBE Mark-1 is designed to collect aerothermal and gas species data of a hypersonic flow environment to improve the understanding of nonequilibrium chemical reaction rates and molecular relaxation rates. This experiment will be conducted in a high Mach number, continuum, nonequilibrium flow regime that exhibits gas dissociation effects within a specified range of altitudes and velocities.

To aid in the design process, high-fidelity numerical methods were employed along with simplified engineering-level estimation tools to evaluate design choices and their effect of vehicle trajectory and expected measurement environments. The simple estimation tool was used to ensure that proposed designs achieved a trajectory that passed through the desired region of interest and to determine whether the desired non-ablative environment would be feasible. The full three-dimensional solutions were then leveraged to facilitate sensor suite design choices, such as sensor measurement range, placement and arrangement, and selection. They were also used to analyze methods of post-flight

data reconstruction.

A key result from this work is the conclusion that the original 3U HyCUBE vehicle concept was incompatible with a non-ablative environment. The stagnation point estimator found that the aerothermal conditions along its trajectory greatly exceeded the rated limits of the proposed non-ablative TUFROC TPS. The proposed redesigned 12U vehicle does comply with a non-ablative environment, which was shown using the stagnation point estimator. Another key result is the development of a sensor suite for the HyCUBE concept. Sensors were identified using the solutions to the high-fidelity CFD to measure pressure, temperature, and gas species composition, and their locations and orientations were also analyzed in an effort to maximize information recovery. Much of the analysis presented in this thesis for the 3U concept will need to be re-done for the 12U concept, so another key result is the development of software tools and design processes needed to evaluate this new concept's performance in the same way as the analysis of the first concept.

6.2 Future Work and Considerations

There are several improvements that could be made to the estimation tool that could further develop its capabilities. First, the incorporation of a variable ballistic coefficient from an aerodynamic coefficient database could help improve the accuracy of simulated trajectories. Next, the estimator uses a exponential model of the atmosphere, which could be replaced with, for instance, the US Standard Atmosphere model [46]. While this would not improve the trajectory predictions (the equations of motion assume an exponential atmosphere), the estimates for density with altitude would improve and thus the estimates for heat flux, temperature and pressure. Another potential improvement would be to add in other heating models such as those used by TRAJ.

As was mentioned in the previous section, there remains a significant amount of analysis to be done on the new 12U concept, namely the high-fidelity CFD analysis that will allow for development of an aerodynamic coefficient database and three-dimensional solutions of the flow around the vehicle. This work will improve the estimates of the

12U vehicle's trajectory and allow for stability analysis to be done. Of course, it will also help inform sensor decisions and changes, as discussed in section 5.8.

Beyond the continuing analysis of the new 12U design, there is also work to be done in finding the optimal TPS material to use. As was mentioned in section 5.2, TUFROC has not been tested with certain types of instrumentation that require a non-intact surface, like the pressure sensors and spectrometer. This means that it is not known how these structures in the TPS would effect TUFROC's performance. Going forward, if the 12U concept is chosen as the top candidate design, there is a possibility of dropping the maximum temperature and pressure even more, which may even allow for the use of a more established non-ablator that may be able to be instrumented more readily. Also, there will need to be analysis completed to analyze the needed thickness of TUFROC, or other candidate TPS, using the FIAT software or similar.

Two preliminary designs for the HyCUBE Mark-1 mission are presented in this thesis, both with benefits and challenges. Neither concept is a final design and both are being considered as potential stepping stones to an ultimate concept. For instance, while the 3U concept will not be able to use a non-ablative TPS, it could be used as a simple proof of concept using an ablative TPS to demonstrate the merits of the more complex 12U design, while still collecting useful ablative flight data as well. Other options are being discussed as well, such as using sub-orbital flights to reduce the intense aerothermal environment and working up to orbital flights, addressing the added complexities that each HyCUBE concept requires in an iterative fashion throughout the process.

Bibliography

[1] Jiang, Z., and Yu, H., "Theories and technologies for duplicating hypersonic flight conditions for ground testing," *National Science Review*, Vol. 4, No. 3, 2017, pp. 290–296.

[2] Gu, S., and Olivier, H., "Capabilities and limitations of existing hypersonic facilities," *Progress in Aerospace Sciences*, Vol. 113, 2020, p. 100607.

[3] Venkatapathy, E., Laub, B., Hartman, G., Arnold, J., Wright, M., and Allen Jr, G., "Thermal protection system development, testing, and qualification for atmospheric probes and sample return missions: Examples for Saturn, Titan and Stardust-type sample return," *Advances in Space Research*, Vol. 44, No. 1, 2009, pp. 138–150.

[4] Banerji, N., "The effects of radiation on ablative heat shields during atmospheric entry," Tech. rep., EPFL, 2017.

[5] Schneider, S. P., "Laminar-turbulent transition on reentry capsules and planetary probes," *Journal of Spacecraft and Rockets*, Vol. 43, No. 6, 2006, pp. 1153–1173.

[6] Wright, M. J., Milos, F. S., and Tran, P., "Afterbody aeroheating flight data for planetary probe thermal protection system design," *Journal of Spacecraft and Rockets*, Vol. 43, No. 5, 2006, pp. 929–943.

[7] Woollard, B. A., Braun, R. D., and Bose, D., "Aerothermodynamic and thermal protection system instrumentation reference guide," *2016 IEEE Aerospace Conference*, IEEE, 2016, pp. 1–22.

[8] Paulat, J., and Boukhobza, P., "Re-entry flight experiments lessons learned - The Atmospheric Reentry Demonstrator ARD," Tech. rep., European Aeronautic Defence and Space Company (EADS), 2007.

[9] Cheatwood, F. M., Bose, D., Karlgaard, C. D., Kuhl, C. A., Santos, J. A., and Wright, M. J., *Mars Science Laboratory (MSL) Entry, Descent, and Landing Instrumentation (MEDLI): complete flight data Set*, National Aeronautics and Space Administration, Langley Research Center, 2014.

[10] Karlgaard, C. D., VanNorman, J., Siemers, P. M., Schoenenberger, M., and Munk, M. M., "Mars entry atmospheric data system modeling, calibration, and error analysis," Tech. rep., National Aeronautics and Space Administration, 2014.

[11] White, T., Mahzari, M., Tang, C., Karlgaard, C. D., Schoenenberger, M., and Cruden, B. A., "The Entry Descent and Landing Instrumentation (MEDLI2) suite for the Mars 2020 mission," *16th International Planetary Probe Workshop*, 2019.

[12] Levin, D. A., Collins, R. J., Candler, G. V., Wright, M. J., and Erdman, P., "Examination of OH ultraviolet radiation from shock-heated air," *Journal of Thermophysics and Heat Transfer*, Vol. 10, No. 2, 1996, pp. 200–208.

[13] Erdman, P. W., Zipf, E. C., Espy, P., Howlett, C. L., Levin, D. A., Collins, R. J., and Candler, G. V., "Measurements of ultraviolet radiation from a 5-km/s bow shock," *Journal of Thermophysics and Heat Transfer*, Vol. 8, No. 3, 1994, pp. 441–446.

[14] Levin, D., Candler, G. V., Collins, R., Erdman, P., Zipf, E., Espy, P., and Howlett, C., "Comparison of theory with experiment for the bow shock ultraviolet rocket flight," *Journal of Thermophysics and Heat Transfer*, Vol. 7, No. 1, 1993, pp. 30–36.

[15] Levin, D. A., Candler, G. V., Collins, R. J., Erdman, P. W., Zipf, E. C., and Howlett, L. C., "Examination of theory for bow shock ultraviolet rocket experiments – I," *Journal of Thermophysics and Heat Transfer*, Vol. 8, No. 3, 1994, pp. 447–452.

[16] Boyd, I. D., Candler, G. V., and Levin, D. A., "Dissociation modeling in low density hypersonic flows of air," *Physics of Fluids*, Vol. 7, No. 7, 1995, pp. 1757–1763.

[17] Levin, D. A., Braunstein, M., Candler, G. V., Collins, R. J., and Smith, G. P., "Examination of theory for bow shock ultraviolet rocket experiments – II," *Journal of Thermophysics and Heat Transfer*, Vol. 8, No. 3, 1994, pp. 453–459.

[18] Boyd, I. D., Phillips, W. D., and Levin, D. A., "Prediction of ultraviolet radiation in nonequilibrium hypersonic bow-shock waves," *Journal of Thermophysics and Heat Transfer*, Vol. 12, No. 1, 1998, pp. 38–44.

[19] Kimmel, R., Adamczak, D., Berger, K., and Choudhari, M., "HIFiRE-5 flight vehicle design," *40th Fluid Dynamics Conference and Exhibit*, 2015, p. 4985.

[20] Kimmel, R., Adamczak, D., Paull, A., Paull, R., Shannon, J., Pietsch, R., Frost, M., and Alesi, H., "HIFiRE-1 preliminary aerothermodynamic measurements," *41st AIAA Fluid Dynamics Conference and Exhibit*, 2011, p. 3413.

[21] Wheaton, B. M., Berridge, D. C., Wolf, T. D., Araya, D. B., Stevens, R. T., McGrath, B. E., Kemp, B. L., and Adamczak, D. W., "Final design of the Boundary Layer Transition (BOLT) flight experiment," *Journal of Spacecraft and Rockets*, Vol. 58, No. 1, 2021, pp. 6–17.

[22] Gülhan, A., Siebe, F., Thiele, T., Neeb, D., Turner, J., and Ettl, J., "Instrumentation of the SHEFEX-II flight experiment and selected flight data," *18th AIAA/3AF International Space Planes and Hypersonic Systems and Technologies Conference*, 2012, p. 5819.

[23] Loomis, M., and Palmer, G., "Pre-flight CFD analysis of arc jet and flight environments for the SHARP-B2 flight experiment," *39th Aerospace Sciences Meeting and Exhibit*, 2001, p. 982.

[24] Gülhan, A., Siebe, F., Thiele, T., Neeb, D., Turner, J., and Ettl, J., "Sharp Edge Flight Experiment-II instrumentation challenges and selected flight data," *Journal of Spacecraft and Rockets*, Vol. 51, No. 1, 2014, pp. 175–186.

[25] "CubeSat 101: Basic concepts and processes for first-time CubeSat developers," Web, 2017. https://www.nasa.gov/sites/default/files/atoms/files/nasa_csli_cubesat_101_508.pdf.

[26] Swei, S. S.-M., and Westfall, A., "Attitude control system design for CubeSats configured with Exo-Brake parachute," *AIAA SPACE 2016*, 2016, p. 5540.

[27] Murbach, M., Guarneros, A., Alena, R., Papadopoulos, P., Tanner, F., Wheless, J., Smith, S., Salas, A., and Williams, N., "The TechEdSat-N series: A collaborative technology development platform in the nano-satellite form factor," 2018.

[28] Murbach, M., "An overview of the SOAREX and TechEdSat flight series: missions to advance re-entry experimentation, planetary mission design, and flight technology," *12th International Planetary Probe Workshop*, 2015.

[29] TechEdSat Team, "Upcoming Exo-Brake and nano-sat advanced flight experiments – TechedSat 6,7,8," 2017.

[30] Sakraker, I., "Aerothermodynamics of pre-flight and in-flight testing methodologies for atmospheric entry probes," Ph.D. thesis, Université de Liège, Liège, Belgique, 2016.

[31] Miccoli, C., "Detailed modeling of cork-phenolic ablators in preparation to the post-flight analysis of the QARMAN re-entry CubeSat," Ph.D. thesis, Politecnico di Torino, 2020.

[32] Masutti, D., Trifoni, E., Umit, E., Martucci, A., Denis, A., Purpura, C., Scholz, T., Ceglia, G., Testani, P., Sakraker, I., et al., "QARMAN re-entry CubeSat: Preliminary results of SCIROCCO plasma wind tunnel testing," *15th International Planetary Probe Workshop Short Course -— Small Satellites: An Emerging Paradigm for Bold Planetary Exploration*, 2018.

[33] Goggin, M., Tamrazian, S., Carlson, R., Tidwell, A., and Parkos, D., "CubeSat sensor platform for reentry aerothermodynamics," 2017.

[34] Morgan, J., Nuwal, N., Williams, J., Putnam, Z. R., Levin, D. A., Pikus, A., Berger, A., and Alexeenko, A., "Prediction of flight measurements of high-enthalpy nonequilibrium Flow from a CubeSat-class atmospheric probe," *2018 AIAA Aerospace Sciences Meeting*, 2018, p. 1234.

[35] Weaver, M., and Ailor, W., "Reentry Breakup Recorder: Concept, testing, moving forward," *AIAA SPACE 2012 Conference & Exposition*, 2012, p. 5271.

[36] Feistel, A. S., Weaver, M. A., and Ailor, W. H., "Comparison of Reentry Breakup measurements for three atmospheric reentries," *6th IAASS Conference*, 2013.

[37] Sidor, A., Braun, R. D., and DePasquale, D., "RED-Data2 commercial reentry recorder: Size reduction and improved electronics design," *AIAA Atmospheric Flight Mechanics Conference*, 2014, p. 1231.

[38] Ehresmann, M., Behnke, A., Baumann, J., Tietz, R., Franz, J., Galla, D., Gäßler, B., Grabi, F., Hessinger, F., Hießl, R., et al., "CubeSat-sized re-entry capsule MIRKA2," *10th IAA Symposium on Small Satellites for Earth Observation*, 2015.

[39] Empey, D., Gorbunov, S., Skokova, K., Agrawal, P., Swanson, G., Prabhu, D., Mangimi, N., Peterson, K., Winter, M., and Venkatapathy, E., "Small Probe Reentry Investigation for TPS Engineering (SPRITE)," *50th AIAA Aerospace Sciences Meeting including the New Horizons Forum and Aerospace Exposition*, 2012, p. 215.

[40] Sparks, J. D., and Martin, A., "Overview of the second test-flight of the Kentucky Re-entry Universal Payload System (KRUPS)," *2018 Joint Thermophysics and Heat Transfer Conference*, 2018, p. 3589.

[41] Sparks, J. D., Whitmer, E. C., Smith, S. W., and Martin, A., "Overview of the first test-flight of the Kentucky Re-entry Universal Payload System (KRUPS)," *2018 AIAA Aerospace Sciences Meeting*, 2018, p. 1720.

[42] Nichols, J. T., "The Kentucky Re-Entry Universal Payload System (KRUPS): Orbital flight," Master's thesis, University of Kentucky, 2021.

[43] Cassell, A., Wercinski, P., Smith, B., Yount, B., Nishioka, O., and Kruger, C., "ADEPT Sounding Rocket One flight test overview," *AIAA Aviation 2019 Forum*, 2019, p. 2896.

[44] Hayes, A. D., Nompelis, I., Caverly, R., Mueller, J., and Gebre-Egziabher, D., "Dynamic stability analysis of a hypersonic entry vehicle with a non-linear aerodynamic model," *AIAA AVIATION 2020 FORUM*, 2020, p. 3201.

[45] Putnam, Z. R., and Braun, R. D., "Extension and enhancement of the Allen-Eggers analytic solution for ballistic entry trajectories," *AIAA Atmospheric FLight Mechanics Conference*, 2014, p. 2381.

[46] *US standard atmosphere*, National Oceanic and Atmospheric Administration, 1976.

[47] Allen, H. J., and Eggers, A. J., "A study of the motion and aerodynamic heating of ballistic missiles entering the earth's atmosphere at high supersonic speeds," *NACA Rept*, Vol. 1381, 1958.

[48] Shampine, L. F., and Reichelt, M. W., "The MATLAB ODE Suite," *SIAM Journal on Scientific Computing*, Vol. 18, No. 1, 1997, pp. 1–22.

[49] Sutton, K., and Graves Jr, R. A., "A general stagnation-point convective heating equation for arbitrary gas mixtures," 1971.

[50] Wright, M., "Aerothermodynamic and thermal protection system aspects of entry system design course," *Short course of the Thermal and Fluids Analysis Workshop (TFAWS) 2012*, 2012.

[51] Stewart, D., and Leiser, D., "Lightweight TUFROC TPS for hypersonic vehicles," *14th AIAA/AHI Space Planes and Hypersonic Systems and Technologies Conference*, 2006, p. 7945.

[52] Kundu, P., Cohen, I., and Dowling, D., *Fluid Mechanics*, Academic Press, 2016, Chap. Conservation Laws.

[53] Allen Jr, G. A., Wright, M. J., and Gage, P., "The trajectory program (traj): Reference manual and user's guide," *NASA TM*, Vol. 212847, 2005.

[54] Loomis, M., and Allen, G., "Demonstration of integrated trajectory/aerothermal/TPS sizing design tools for Mars Smart Lander," *AIAA Atmospheric Flight Mechanics Conference and Exhibit*, 2002, p. 4508.

[55] Saunders, D. A., "Traj_opt user's guide," , 2005.

[56] Brandis, A. M., and Johnston, C. O., "Characterization of stagnation-point heat flux for earth entry," *45th AIAA Plasmadynamics and Lasers Conference*, 2014, p. 2374.

[57] Fay, J. A., and Riddell, F. R., "Theory of stagnation point heat transfer in dissociated air," *Journal of the Aerospace Sciences*, Vol. 25, No. 2, 1958, pp. 73–85.

[58] Gao, D., Zhang, C., and Schwartzentruber, T., "A three-level Cartesian geometry-based implementation of the DSMC method," *48th AIAA Aerospace Sciences Meeting Including the New Horizons Forum and Aerospace Exposition*, 2010, p. 450.

[59] Gao, D., and Schwartzentruber, T. E., "Optimizations and OpenMP implementation for the direct simulation Monte Carlo method," *Computers & Fluids*, Vol. 42, No. 1, 2011, pp. 73–81.

[60] Nompelis, I., and Schwartzentruber, T. E., "Strategies for parallelization of the DSMC method," *51st AIAA Aerospace Sciences Meeting including the New Horizons Forum and Aerospace Exposition 2013*, 2013.

[61] Nompelis, I., Drayna, T. W., and Candler, G. V., "A parallel unstructured implicit solver for hypersonic reacting flow simulation," *Parallel Computational Fluid Dynamics 2005*, Elsevier, 2006, pp. 389–395.

[62] Candler, G. V., Johnson, H. B., Nompelis, I., Gidzak, V. M., Subbareddy, P. K., and Barnhardt, M., "Development of the US3D code for advanced compressible

and reacting flow simulations," *53rd AIAA Aerospace Sciences Meeting*, 2015, p. 1893.

[63] Johnstone, A., "CubeSat design specification Rev. 14." *The CubeSat Program, California Polytechnic State University*, 2020.

[64] Feldman, J., Stewart, D., Leiser, D., Switzer, M., Gokcen, T., and Skokova, K., "TUFROC thermal protection system," *2019 Hypersonic Technology & Systems Conference (HTSC)*, 2019.

[65] Johnson, S., Gasch, M., Leiser, D., Stewart, D., Stackpool, M., Thornton, J., and Espinoza, C., "Development of new TPS at NASA Ames Research Center," *15th AIAA International Space Planes and Hypersonic Systems and Technologies Conference*, 2008, p. 2560.

[66] Chen, Y.-K., and Milos, F. S., "Ablation and thermal response program for spacecraft heatshield analysis," *Journal of Spacecraft and Rockets*, Vol. 36, No. 3, 1999, pp. 475–483.

[67] Park, R. M., "Thermocouple fundamentals," *Course Tech., Temp*, 2010, pp. 2–1.